Studies of F^{18} from the $O^{16}(He^3,p\gamma)F^{18}$ Reaction*

J. W. Olness and E. K. Warburton
Brookhaven National Laboratory, Upton, New York
(Received 16 June 1966)

The Doppler-shift attenuation method was used to investigate the lifetimes of various gamma-ray-emitting states of F^{18} populated via the $O^{16}(He^3,p\gamma)F^{18}$ reaction at a He^3 bombarding energy of 3.4 MeV. Gamma-ray spectra were measured with a lithium-drifted germanium spectrometer for detection angles $\theta_\gamma=8°$ and $\gamma_\gamma=172°$ relative to the incident beam direction. The results determine the mean lifetimes (in picoseconds) for the levels of F^{18}, identified by their excitation energies (in MeV) as follows: 1.70 (0.86 ± 0.20); 2.10 (4.1 ± 1.6); 2.53 (0.67 ± 0.18); 3.06 (<0.17); 3.35 (0.46 ± 0.10); and 3.84 (<0.073). For each of the four longer-lived levels, the mean life was also determined from a theoretical fit to the experimental line shapes; these results have been incorporated in the values quoted for the 1.70-, 2.10-, 2.53-, and 3.35-MeV levels. The particle-gamma angular-correlation method of Litherland and Ferguson was used to gain information on the decay modes and spin assignments of the levels of F^{18} below an excitation energy of 3.4 MeV. Protons were detected with an annular counter at 180° to the He^3 beam and gamma rays were detected at several angles between 0° and 90° to the beam. Measurements were carried out for He^3 bombarding energies of 3.44, 4.65, and 5.40 MeV. These results establish spin assignments of $J=2$ for both the 2.10- and 3.06-MeV levels of F^{18}, and are consistent with or confirm previously established spin-parity assignments for the remaining levels as follows: 0.937 (3^+), 1.70 (1^+), 2.53 (2^+), 3.13 (1), and 3.35 (2 or 3). It is further established that the 2.10- and 1.08-MeV levels have the same parity. The most probable spin of the 1.08-MeV level is found to be $J=0$ (although $J=1$ or 2 are not excluded) in which case the lifetime determined for the 2.10-MeV level establishes that the $2.10\rightarrow1.08$ transition are an enhanced $E2$ of strength approximately 20 Weisskopf units. Additional information was obtained for the mixing ratios of various ground-state and cascade transitions in F^{18}.

I. INTRODUCTION

THE previously available information on the levels of F^{18} below 3.4-MeV excitation has been adequately summarized in a recent publication by Poletti and Warburton[1] in which they report on an investigation of proton-gamma correlations in the $O^{16}(He^3,p\gamma)F^{18}$ reaction. Their conclusions on the spins, parities, and gamma-branching ratios of the first 10 levels of F^{18}, based on their work and the references cited therein, are illustrated by the F^{18} level diagram of Fig. 1 which is taken from their report. Chasman, Ristinen, Jones, and Warburton[2] have more recently reported a precision determination of gamma-ray energies from the above reaction as obtained with a gas target of O^{16} and a lithium-drifted germanium [Ge(Li)] detector. This latter investigation confirms the findings of Poletti and Warburton that the 2.10-MeV level decays primarily to the 0.94- and 1.082-MeV levels. In addition, an upper limit of 6% was placed on possible decays to the 1.045-MeV level.[2] The weighted average of these determinations[1,2] yield revised branching ratios for the 2.10-MeV level of $(38\pm3)\%$, $(30\pm4)\%$, and $(32\pm4)\%$ for transitions to the ground state and to the 0.94- and 1.082-MeV levels, respectively.[2]

In the present paper we report on an extension of these measurements of the $O^{16}(He^3,p\gamma)F^{18}$ reaction ($Q=2.012$ MeV) which was designed in particular to determine the spins of the 2.10- and 3.06-MeV levels of F^{18} for which definite assignments have not been previously given. In Sec. II we consider the results of Doppler shift measurements, made with a Ge(Li) detector, which were undertaken in order to determine or set limits on the lifetimes of those states of interest here. These results are to be compared with the previous measurements of Litherland, Yates, Hinds, and Eccleshall[3] who have studied the 0.94-, 1.04-, 1.08-, 1.70-, 2.10-, and 2.53-MeV levels, employing NaI(Tl) spectroscopy to measure Doppler shifts in the $H^3(O^{16},F^{18})n$ reaction. Some question has been previously raised[2] concerning the lifetime of the 2.10-MeV level, the indications being that the level has a mean life longer than the value $\tau=(0.7\pm0.2)\times10^{-12}$ sec quoted by Litherland *et al.*[3]

In Sec. III we report on the investigation of p-γ correlations, with protons detected in a collinear geometry (i.e., $\theta_p\sim180°$) undertaken to investigate the spins of these F^{18} levels. It is, of course, expected that the lifetime measurements will be useful in considering the effects of multipole mixtures in the gamma-ray correlations studied.

II. DOPPLER-SHIFT MEASUREMENTS

A. Experimental Procedure

Levels of F^{18} were populated via the $O^{16}(He^3,p\gamma)F^{18}$ reaction by 3.4-MeV He^3 bombardment of thick quartz (SiO_2) targets. Gamma rays were detected with a Ge(Li) detector which has been described in detail

* Work performed under the auspices of the U. S. Atomic Energy Commission.
[1] A. R. Poletti and E. K. Warburton, Phys. Rev. 137, B595 (1965).
[2] C. Chasman, K. W. Jones, R. A. Ristinen, and E. K. Warburton, Phys. Rev. 137, B1445 (1965).
[3] A. E. Litherland, M. J. L. Yates, B. M. Hinds, and D. Eccleshall, Nucl. Phys. 44, 220 (1963).

previously,[2,4] as have also the techniques used in the measurement and analysis of the gamma-ray Doppler shifts.[4,5] The detector had a sensitive volume of ~3.5 cm^3, and was housed in an aluminum casing (0.03-in. wall thickness) and cooled to liquid nitrogen temperatures. The targets were identical discs of 1-mm-thick quartz positioned at opposite ends of a 50-cm beam tube, with the Ge(Li) detector located midway between them at a distance of 3.6 cm between the beam axis and the central region of the detector. The target nearest the accelerator (fore-position) was mounted on a movable arm which could be moved into the beam path and out again, thus changing the reaction site from the forward position to the backward position. It was thus possible to study in sequence the spectrum of gamma rays emitted in the forward direction ($\theta_\gamma=8°$) and in the backward direction ($\theta_\gamma=172°$) without disturbing the detector position. Pulses from the detector were amplified with an ORTEC Model 105-XL preamplifier and an ORTEC Model 220 post-bias amplifier with conditions of gain and bias adjusted for the various runs so that the regions of particular interest were displayed across the range of a 1024-channel slice of a TMC-16384 channel analyzer. A precision pulse generator was adjusted to provide a reference peak as a check on possible gain shifts.

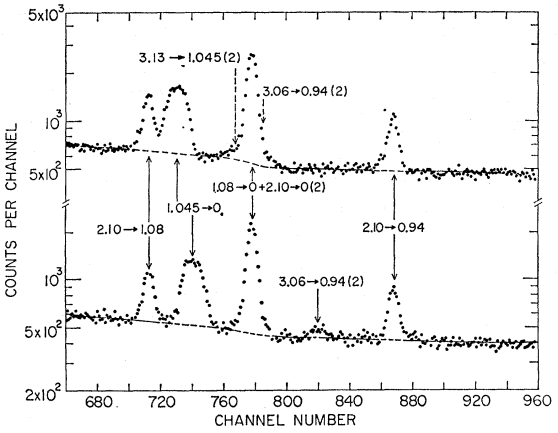

FIG. 2. Partial spectrum of gamma rays from the $O^{16}(He^3,p\gamma)F^{18}$ reaction measured with a Ge(Li) detector, at a bombarding energy of $E_{He^3}=3.4$ MeV. The upper curve is for a detection angle, relative to the incident beam direction, of $\theta_\gamma=172°$ while the lower curve is for $\theta_\gamma=8°$. The arrows indicate the centroids of the various peaks, which are identified according to the excitation energies of the initial and final states of F^{18} between which the transitions occur. Broken arrows indicate uncertain assignments. The numbers in parentheses differentiate between the full-energy peaks (0 or unmarked) and the one-escape and two-escape peaks which may also be observed. These data are part of a 1024-channel spectrum, and cover the region $400\leq E_\gamma\leq 1300$ keV, with a dispersion of 0.923-keV/channel.

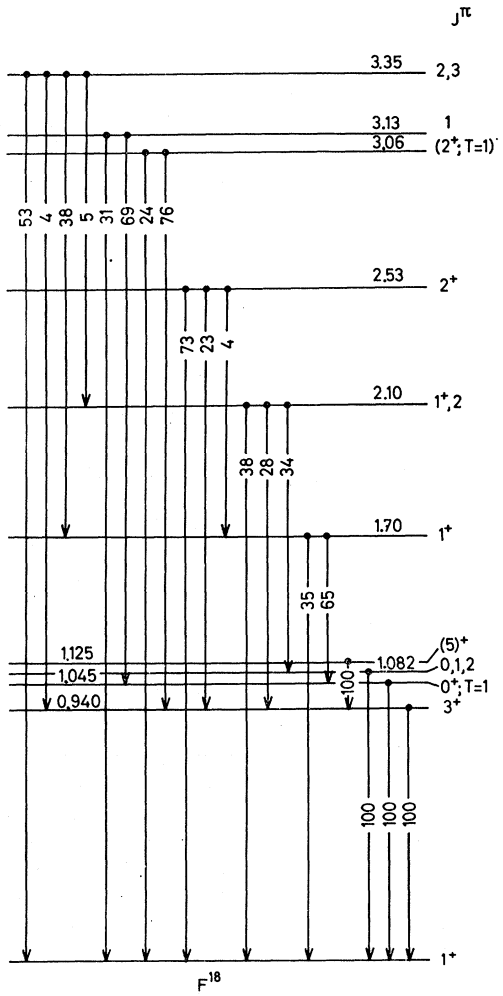

FIG. 1. Level diagram summarizing previously available information on spins, parities, and decay modes of the first 10 levels of F^{18}. The $T=1$ levels are indicated, all other levels are expected to have $T=0$. This figure is taken from the summary of A. R. Poletti and E. K. Warburton [Phys. Rev. **137**, B595 (1965)] and is based on their investigation of the $O^{16}(He^3,p\gamma)F^{18}$ reaction together with the prior information referenced therein.

The results of one such measurement are shown in Fig. 2. In this case, the analyzer was set to record the spectrum corresponding to the region $400\leq E_\gamma\leq 1300$ keV at a dispersion of 0.923-keV/channel. The upper curve shows the spectrum measured for $\theta_\gamma=172°$ for a bombardment of ~10 000 μC. The lower curve shows the sum of two measurements for $\theta_\gamma=8°$, each for a bombardment of ~5000 μC, which were recorded just before and just after the data of the upper curve. This procedure was also used for subsequent measurements, since it permitted a convenient check on the stability of the system, and also since the effects of long-term drifts in gain would be to some extent reduced by this procedure.

All of the lines labeled in Fig. 2 are due to transitions in F^{18}, and are labeled according to the energies (in MeV) of the initial and final levels between which the transitions take place. The energy calibration is based

[4] E. K. Warburton, J. W. Olness, K. W. Jones, C. Chasman, R. A. Ristinen, and D. H. Wilkinson, Phys. Rev. **148**, 1072 (1966).
[5] E. K. Warburton, D. E. Alburger, and D. H. Wilkinson, Phys. Rev. **129**, 2180 (1963).

on the position of the 511-keV annihilation peak (not shown in Fig. 2) and on subsequent calibration measurements with a ThC″ source and a precision pulser.

The narrow lines evident in Fig. 2 exhibit a breadth characteristic of the detector resolution, while the breadth of the broader lines is clearly influenced by the recoil angular distribution and/or the nuclear lifetimes (i.e., Doppler effects). A procedure which has been described previously[4] was therefore adopted to determine the "centroids" of the various line shapes. In this procedure an exponential "background," as determined by a least-squares fit to the data away from the peak region, is subtracted from the peaks of interest and the centroid of the resultant distribution is computed. For the narrow symmetric peaks a Gaussian fit was also made. The centroids thus determined have net uncertainties of $\lesssim 1$ channel, and are indicated by the arrows in Fig. 2. Those lines which could be identified positively and most accurately were used to provide internal calibration points for the final determination of energies. (Note that the average value of the centroid energy, i.e., for $\theta_\gamma=8°$ and $\theta_\gamma=172°$, defines the transition energy $E_{\gamma 0}$.) The sum total of calibration data was then used to find the coefficients for a polynomial fit to the data given by

$$E_\gamma=\sum_{\nu=0}^{n} a_\nu x^\nu, \qquad (1)$$

where x is the channel number and n was varied from 1 to 3. The results indicate, as based on the examination of the χ^2 values for the above solutions, that there was no significant deviation from the linear relationship $E_\gamma=a_0+a_1x$.

An analogous presentation is given in Fig. 3 for the energy region 1430–1760 keV, with a dispersion of 1.323 keV/channel. Figure 4 shows a continuation of the plot presented in Fig. 3 covering in this case the energy region 1970–2420 keV. Also shown in Fig. 3 is a portion of a spectrum showing the full energy peak of the $2.53\rightarrow 0$ transition, which exhibits the same peculiar shape found for the two-escape peak of the $2.53\rightarrow 0$ transition.

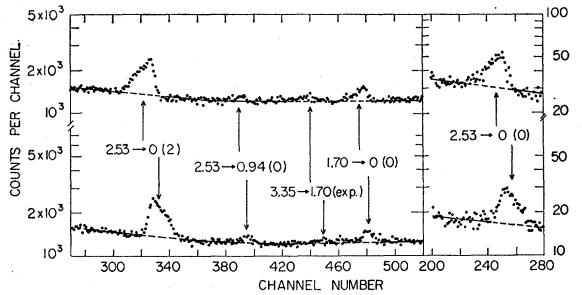

FIG. 3. Partial spectrum of gamma rays from the $O^{16}(He^3,p\gamma)F^{18}$ reaction measured at $E_{He^3}=3.4$ MeV with a Ge(Li) detector. The presentation is analogous to that of Fig. 2. The upper curve is for a detection angle $\theta_\gamma=172°$ while the lower curve is for $\theta_\gamma=8°$. These spectra include the energy region $1430\leq E\leq 1760$ keV and were measured with a dispersion of 1.323 keV/channel. The insert shows that the full-energy peak of the $2.53\rightarrow 0$ transition exhibits a structure similar to that observed for the two-escape peak of this transition.

Comparing the data of Figs. 2, 3, and 4 for $\theta_\gamma=172°$ (upper curves) and $\theta_\gamma=8°$ (lower curves), it is readily apparent that transitions from the 3.06- and 1.045-MeV levels exhibit a large percentage shift in energy as compared to the shifts observed for the 3.35-, 2.53-, 2.10-, and 1.70-MeV levels, while transitions from the 1.08-MeV level and the 0.94-MeV level (not shown) exhibit no detectable shift. The suggestion, of course, is that the second group of levels have lifetimes comparable to the stopping time of F^{18} ions in the target material, SiO_2, while the first and third groups, respectively, have lifetimes appreciably shorter than, and longer than, this slowing down time. It is the purpose of the following analyses to provide a quantitative interpretation of these observations in order to determine or set limits on the lifetimes of these nuclear levels.

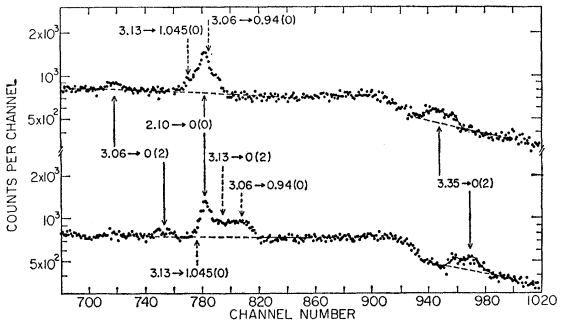

FIG. 4. Partial spectrum of gamma rays from the $O^{16}(He^3,p\gamma)F^{18}$ reaction measured at $E_{He^3}=3.4$ MeV with a Ge(Li) detector. The presentation is analogous to that of Figs. 2 and 3. The upper curve is for a detection angle of $\theta_\gamma=172°$, while the lower curve is for $\theta_\gamma=8°$. These data are a continuation of the plot shown in Fig. 3, and cover the energy region from 1970 to 2420 keV.

B. Method of Analysis

Applications of the Doppler shift attenuation method have been described in some detail previously.[3–5] The general procedure, which we have also followed here, is to extract from the data on a given transition an experimentally determined value of the attenuation factor F'. This value is then compared with the values $F(\tau)$ predicted theoretically for various mean lifetimes τ, and thus the lifetime of the emitting level is ascertained. [We follow previous notation[4,5] in using a prime to designate the experimentally determined quantity F' as being distinct from the theoretically predicted values $F(\tau)$.]

Although the dependence of the Doppler-shifted line shape upon the nuclear lifetime is necessarily implicit in the equations which are applied to this approach, only the information contained in the centroid shift is actually evaluated. In earlier experiments utilizing NaI(Tl) spectroscopy, this restriction was imposed by the fact that the detector resolution function was much

broader than the line shape. With the excellent resolution of presently available Ge(Li) detectors, this restriction no longer applies. Accordingly, we describe an alternative approach to the evaluation of the Doppler shift data, in which the nuclear lifetimes are determined through a comparison of the experimentally determined line shapes and those predicted theoretically for various assumed lifetimes. For the purpose of illustrating the latter procedure, it is useful here to review briefly the approach of the Doppler-shift attenuation method.

The Doppler-Shift Attenuation Method

The average (or centroid) energy of the de-excitation gamma rays emitted by an ensemble of recoil nuclei formed in a reaction induced by particle bombardment is given[4,5] by

$$\langle E_\gamma\rangle = E_{\gamma 0}[1+F(\tau)\langle\beta(0)\rangle\cos\theta], \tag{2}$$

where $E_{\gamma 0}$ is the gamma radiation energy for nuclei at rest, and θ specifies the direction of gamma emission relative to the axis defined by the bombardment (the z axis). $\langle\beta(t=0)\rangle$ is the average component along this z axis of the initial recoil ion velocity, corresponding to the individual times of formation defined at $t=0$. $F(\tau)$ is the Doppler-shift attenuation factor whose deviation from unity $[0\leq F(\tau)\leq 1]$ expresses the effect on $\langle E_\gamma\rangle$ due to slowing down of the emitting nuclei in the stopping medium.

The experimental method which we have used here is to measure the Doppler-induced shift $\langle\Delta E_\gamma\rangle$ corresponding to two detection angles θ_1 and θ_2, namely,

$$\langle\Delta E_\gamma\rangle = \{\langle E_\gamma(\theta_1)\rangle - \langle E_\gamma(\theta_2)\rangle\}. \tag{3}$$

For this case then F' is simply

$$F' = \frac{\langle\Delta E_\gamma\rangle}{E_{\gamma 0}\langle\beta(0)\rangle(\cos\theta_1-\cos\theta_2)}. \tag{4}$$

The denominator may be recognized as the shift which would be obtained in the event the lifetime is very much less than the ion stopping time. It must be assumed, of course, that the value of $\langle\beta(0)\rangle$ can be specified, either through the restrictions imposed by the reaction kinematics, or through coincidence techniques using a particle detector to define an appropriate range of recoil momenta. (We note that the equations herein assume an axially symmetric distribution of reaction products, which condition must be preserved by the coincidence particle detection.)

It has been shown previously[4] that an analytic relationship between the attenuation factor $F(\tau)$ and the lifetime τ can be given for particular choices of a phenomenological representation of the slowing down process. The appropriate curve of (dE/dx) versus E for the slowing down of F^{18} ions in quartz (SiO_2) is shown in Fig. 5. In this case we have plotted dE/dx

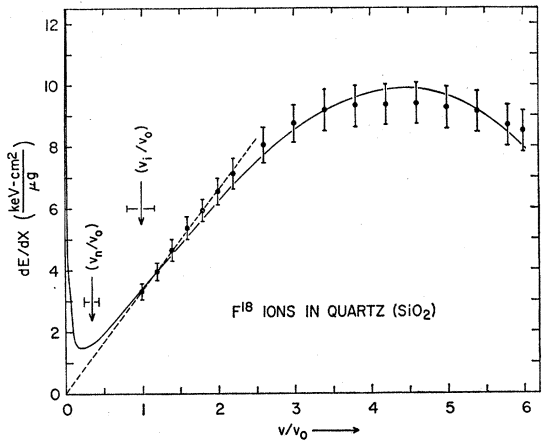

FIG. 5. Plot of dE/dx versus v for F^{18} ions slowing down in a quartz (SiO_2) medium. The F^{18} ion velocity is given in units of $v_0=c/137$. The points are obtained through extrapolation procedures from published experimental data; the errors incorporate the net uncertainty attached both to the original data and to the extrapolation procedures, as explained in the text. The solid curve shows a fit to the data of the form $dE/dx=K_n(v/v_0)^{-1}+K_e(v/v_0)-K_3(v/v_0)^3$ with $K_n=0.164$, $K_e=3.30$, and $K_3=0.055$. The dashed curve is for $K_n=K_3=0$. The initial F^{18} ion velocity v_i computed from the kinematics for the $O^{16}(He^3,p\gamma)F^{18}$ reaction, assuming an isotropic distribution of outgoing protons, is indicated.

(in keV cm^2/μg) versus the ratio v/v_0, where v is the ion velocity and $v_0\equiv c/137$. (Note that $v/v_0=\beta/\beta_0$.) The dots show the values obtained through extrapolation procedures from experimental data[6] for the range and/or energy loss of various ions in various stopping materials, while the error bars indicate the over-all uncertainty associated with both the data and the extrapolation procedure. These data were principally for the stopping of H^1, O^{16}, and Ne^{20} ions in C^{12}, Al^{27}, and Ni^{58}.[6] The solid curve shows the fit to the data generated with the phenomenological relationship[4]

$$dE/dx=K_n(v/v_0)^{-1}+K_e(v/v_0)-K_3(v/v_0)^3, \tag{5}$$

where

$$K_n/K_e=\frac{4}{\pi^2}(v_n/v_0)^2 \tag{6}$$

defines the ratio (v_n/v_0). This ratio determines the importance at small velocities of the nuclear stopping and scattering ($\propto K_n$) relative to the electronic stopping ($\propto K_e$). It is relatively insensitive to the combination of recoil-ion and stopping material and a value $(v_n/v_0)=(0.35\pm0.10)$ was readily extracted from range versus velocity curves for similar combinations. It is important to stress that K_n expresses the full effect of the nuclear

[6] The following review article was particularly useful: W. Whaling, in *Handbuch der Physik*, edited by S. Flügge (Springer-Verlag, Berlin, 1937), Vol. 34. Data on which the extrapolations are based were taken primarily from the following sources: D. I. Porat and K. Ramavataram, Proc. Roy. Soc. (London) **A252**, 394 (1959); D. I. Porat and K. Ramavataram, Proc. Phys. Soc. (London) **77**, 97 (1961). The general procedures are discussed by Warburton *et al.* in Ref. 5 of this paper.

stopping process, and includes the effect of direction changes as well as energy losses in the scattering process. This is so because the range-energy data from which K_n was obtained is for *projected* ranges, and *not* for path lengths in the stopping material.

The significance of the various terms are discussed with reference to Eq. (1) of Ref. 4. The fit to the data is entirely satisfactory for our present purposes, and we shall henceforth assume the dependence given by the analytic expression dE/dx versus v. The characteristic stopping time α has been thus defined as $\alpha=Mv_0/K$, where $K=(K_e^2+4K_nK_3)^{1/2}$ and M is the moving-ion mass. A general relationship between $F(\tau)$ and the ratio α/τ has been given previously [Eq. (4), Ref. 4]. In the present experiment the reaction kinematics restricts the range of initial ion velocities v_i to the region $v_i/v_0 \lesssim 1$. Within this region the K_3 term of Eq. (5) can be neglected. The relationship between $F(\tau)$ and τ is then given by

$$F(\tau)=\left(\frac{\lambda\alpha}{1+\lambda\alpha}\right)(1-\delta(\gamma_i)), \tag{7}$$

where $\lambda=1/\tau$ and $\gamma_i=(\pi/2)v_i/v_n$. Here $\delta(\gamma_i)$ is a calculable function of γ_i (equal to 0 for $K_n=0$) and depends also on $\lambda\alpha$ as discussed previously.[5] The procedure adopted in the following analysis of the Doppler shift attenuation was to calculate a family of curves, corresponding to various values of γ_i, of $F(\tau)$ versus $\lambda\alpha$. In this way a graphical solution for the product $\lambda\alpha$ could be readily obtained for the experimentally determined values of F'.

Analysis of the Line Shapes

It is of course clear from the above presentation that, for a given gamma-ray transition, the Doppler effect gives rise to a distribution of energies resulting in a line shape characteristic of the nuclear lifetime τ and the slowing-down time α of the stopping medium. The line shape will naturally be broadened to some extent according to the reaction kinematics, owing in particular to the spread in energy and angle of the ensemble of recoil ions. For cases where the effects of these spreads are not too severe, it should in principle be possible to extract the nuclear lifetime from the measured line shape. This problem has been discussed previously by Litherland *et al.*[3] who have illustrated numerical solutions of the general equations for particular examples.

In particular, since there is a linear relation between the gamma ray energy E_γ and the nuclear recoil velocity v, the spectral shape can be directly related to the frequency distribution $dN(v)/dv$ where v refers to the ion velocity at the moment of gamma-ray emission. For the moment it is convenient to consider an "idealized" case of gamma emission from ions of uniform initial velocity v_i coming to rest in a stopping medium characterized by the dE/dx relationship given by Eq. (5). In practice this would be obtained by using a thin target, thus fixing the effective bombarding energy within rather small limits, and by using a coincidence particle detector to fix the recoil direction. A general expression thus obtained for the frequency distribution of gamma rays emitted as a function of ion velocity $V\equiv v/v_i$ is given by

$$\frac{dN(V)}{dV}=\left(\frac{\lambda\alpha}{v_i}\right)\left(\frac{v}{v_i}\right)^{\lambda\alpha-1} \times\frac{[\gamma_i^2/(1+\gamma_i^2)]^{\frac{1}{2}\lambda\alpha}[1+\gamma_i^{-2}(v_i/v)^2]^{\frac{1}{2}\lambda\alpha-1}}{(1+C_i)^{\frac{1}{2}\lambda\alpha}\{1-[C_i/(1+C_i)](v/v_i)^2\}^{\frac{1}{2}\lambda\alpha+1}} +\frac{\delta(v/v_i)}{(1+\gamma_i^2)^{\frac{1}{2}\lambda\alpha}}, \tag{8}$$

where

$$C_i=\frac{K-K_e+2K_3(v_i/v_0)^2}{K+K_e-2K_3(v_i/v_0)^2} \tag{9}$$

and $\delta(v/v_i)$ is a delta function of v/v_i. For the case in which we are limited to the region where we can set $K_3=0$, then $C_i\to 0$ and the relationship simplifies to the form,

$$\frac{dN(V)}{dV}\propto\left\{\frac{\alpha}{\tau}V\left[V^2+\frac{1}{\gamma_i^2}\right]^{(\alpha/2\tau)-1}+\frac{1}{(\gamma_i^2)^{\alpha/2\tau}}\delta(V)\right\}. \tag{10}$$

The first term goes to zero as $V\to 0$, and describes the contribution to the net spectrum of those transitions which occur while the emitting nucleus is in motion, i.e., $V>0$. We shall refer to this as the fast component,

$$N_f'(V)=(dN(V)/dV)_f.$$

The second term comprises the contribution of those transitions which occur after the emitting nucleus has come to rest, i.e., $V\sim 0$. Its presence derives largely from the nuclear stopping power $(dE/dx)_n$ which is steeply rising for $v<v_n$. (The implication of course is that the time required for the ion to be degraded from a velocity $v\sim v_n$ to $v\sim 0$ is very small.) We shall refer to this "stopped" component corresponding to $V\sim 0$, as

$$N_s'(V)=(dN(V)/dV)_s.$$

For the present experiment (F^{18} ions stopping in quartz) $v_n/v_0\sim 0.35\pm 0.10$ and $\gamma_i^2=[\frac{1}{2}\pi(v_i/v_n)]^2\cong 20$. Using these values, the first term of Eq. (10) [corresponding to the "fast" component $N_f'(V)$] is plotted in Fig. 6(a) as a function of $V=v/v_i$ for various values of α/τ. In Fig. 6(b) is plotted the ratio,

$$R\equiv\frac{I_s}{I_f}=\frac{1}{(\gamma_i^2+1)^{\alpha/2\tau}-1}, \tag{11}$$

where I_s and I_f are the integrated intensities of the "stopped" and "fast" components, respectively. The spectral shapes characteristic of various values of α/τ

are readily inferred from the curves of Fig. 6. For values $\alpha/\tau \ll 1$ the intensity is all in the stopped peak at $v/v_i=0$. For $\alpha/\tau \gg 1$ the intensity is all in the fast peak which decays exponentially from a maximum at $v/v_i=1$. For intermediate values of α/τ there will be a distribution of intensities given by the ratio R of Fig. 6(b), while the shape of the fast component is given by the appropriate curve of Fig. 6(a). The application of these equations is illustrated by several examples in the following presentation of the results of this analysis.

Evaluation of the Average Recoil Velocity

In the present analysis the determination of the average initial ion velocity $\langle\beta(0)\rangle$ is complicated by the fact that we have used a thick target, and thus must deal with a finite range of bombarding energies, and have also an unknown angular distribution of recoil nuclei. This problem has been discussed more fully with reference to Eqs. (6)–(9) of Ref. 5.

The initial values of the z components of the ion velocities are given by

$$\beta(0)=\beta_{\text{c.m.}}+\beta_R\cos\theta_{\text{c.m.}}, \tag{12}$$

where $\beta_{\text{c.m.}}$ is the laboratory velocity of the center of mass and β_R is the center-of-mass velocity of the recoiling nucleus moving at an angle $\theta_{\text{c.m.}}$ with respect to the z axis.

We have estimated $\langle\beta(0)\rangle$ assuming a center-of-mass distribution of recoil nuclei corresponding to $\langle\cos\theta_{\text{c.m.}}\rangle = 0.0\pm0.33$, and an initial velocity of the center of mass given by

$$\beta_{\text{c.m.}}=\frac{1}{c}\int v\times\sigma(E)\left(\frac{dE}{dx}\right)^{-1}dv \Big/ \int\sigma(E)\left(\frac{dE}{dx}\right)^{-1}dv. \tag{13}$$

The dependences of $\sigma(E)$ on E [and hence on $v=(2ME)^{1/2}$] were taken from the 90° $O^{16}(He^3,p)F^{18*}$ cross section data of Kuehner, Almqvist, and Bromley[7] for production of groups $p_{1,2,3,4}$ (unresolved) and also p_5, p_6, and p_7. Since their curves extend only from 2.1 to 3.2 MeV it was necessary to extrapolate the generally rising cross section to 3.4 MeV, and a 30% uncertainty was assigned to this extrapolation. The energy dependence of dE/dx for He^3 ions in quartz was extrapolated from the data summarized by Whaling.[6] [Note that the factor $(dE/dx)^{-1}$ effectively reduces the importance of the nonzero cross sections for $E<2$ MeV.] The results indicate for $\langle\beta_{\text{c.m.}}\rangle$ a value corresponding to an average bombarding energy of (2.9±0.15) MeV. The uncertainty has been set large enough to cover the calculated variation for the 7 groups thus studied, and is expected to encompass also the proper values for groups p_8, p_9, and p_{10} which are of interest here.

β_R was then calculated from the reaction kinematics using this average value for $\beta_{\text{c.m.}}$ corresponding to $E_{He^3}=2.9$ MeV.

We note here that some justification for the assump-

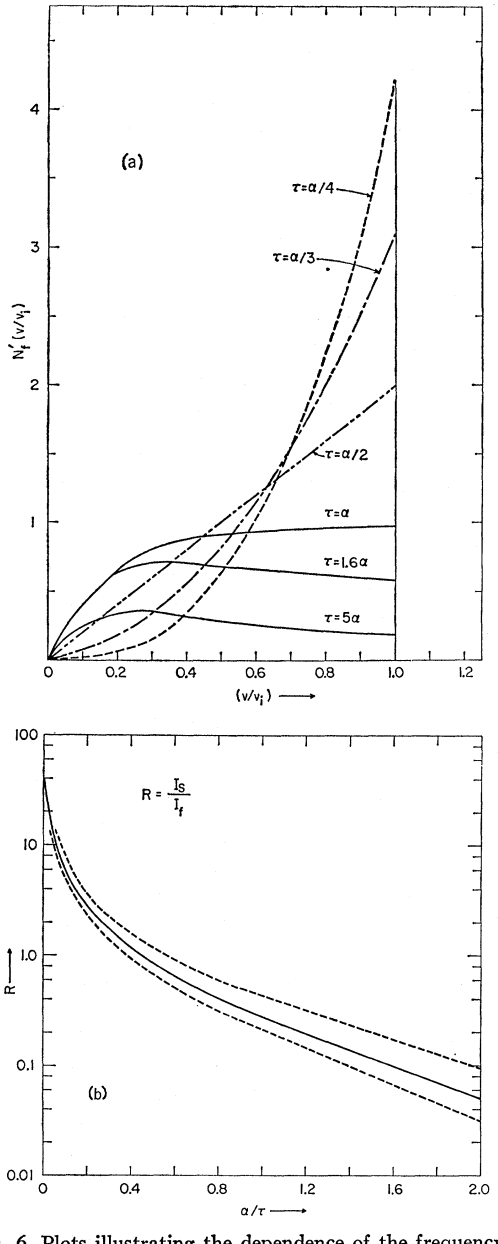

FIG. 6. Plots illustrating the dependence of the frequency distribution $dN(V)/dV=[N_f'(V)+N_s'(V\sim0)]$ upon the nuclear lifetime τ and the stopping time α characteristic of the slowing down medium. $dN(V)/dV$ gives specifically the number of gamma rays emitted from ions of velocity $\sim V$ in the interval dV, while $N_f'(V)$ and $N_s'(V\cong0)$ are, respectively, the fast and slow components defined in the text. Since there is a linear relation between the ion velocity and the Doppler-shifted gamma energy, these curves also predict the shape of the Doppler-shifted gamma-ray lines. The upper curves show the shape of this fast component $N_f'(V)$ as a function of $V\equiv(v/v_i)$ calculated for various values of the ratio α/τ. The lower plot shows how the intensity ratio of these two components varies as a function of the ratio α/τ. These curves were calculated for the $O^{16}(He^3,p\gamma)F^{18}$ reaction at a He^3 bombarding energy of 3.4 MeV.

[7] J. A. Kuehner, E. Almqvist, and D. A. Bromley, Phys. Rev. 122, 908 (1961).

tion $\langle\cos\theta\rangle = 0.0 \pm 0.33$ is found in the measured angular distributions for proton groups p_0, p_5, and p_6 which correspond[7] to values of $\langle\cos\theta\rangle$ well within the assumed limits, and also from the gamma-ray spectra of Figs. 2, 3, and 4 in which the peak widths for those transitions for which, (as will be shown) $\tau < \alpha$, are consistent with values $\langle\cos\theta\rangle \sim 0$.

C. RESULTS

The values of the attenuation factor F' determined from the analysis of the data illustrated in Figs. 2, 3, and 4 are summarized in column 4 of Table I. The measured shifts $\langle\Delta E_\gamma\rangle_{\text{expt}}$ corresponding to the various transitions studied are listed in column 2, while the expected shifts computed from the kinematics for $\tau \ll \alpha$, corresponding to the denominator of Eq. (4), are summarized in column 3. The values of the initial ion velocities v_i/v_0 used in these calculations are listed in column 5. Under the assumptions outlined in Sec. IIB the initial ion velocities are all assumed to be identical. The uncertainty in v_i/v_0 is then roughly proportional to the second term of Eq. (12), since the uncertainty assigned to $\langle\cos\theta_{\text{c.m.}}\rangle = 0 \pm 0.33$ dominates the over-all uncertainty in v_i/v_0. Since this term is also proportional to β_R, however, its relative importance decreases with increasing excitation energy in F^{18}. The listed uncertainties in v_i/v_0 also include the uncertainty associated with the evaluation of the effective bombarding energy.

Solutions for the product $\lambda\alpha$ corresponding to the experimentally determined values F' were then obtained, as explained previously, from the plots of $F(\tau)$ versus $\lambda\alpha$. The solutions for τ corresponding to a stopping time $\alpha = (4.67 \pm 0.7) \times 10^{-13}$ sec appropriate to the dE/dx data of Fig. 5 are indicated in column 6 of Table I.

With reference to Table I, we note that the $3.06 \rightarrow 0$ transition exhibits a Doppler shift consistent with an attenuation factor $F' \cong 1$. Hence we are only able to set the indicated lower limit (to two standard deviations) on the lifetime of the 3.06-MeV level. Again, the 1.045-MeV level is known to be populated to some extent by transitions from longer lived, higher lying levels, for example, the 34% branch from the 2.10-MeV level, and hence we obtain only a lower limit for F'. The corresponding limit on τ is consistent with previous determinations which yield $\tau < 3 \times 10^{-13}$ sec. Also included in Table I is the Doppler shift information on the 3.83-MeV level of F^{18}, this being one of the triplet of levels at 3.73, 3.79, and 3.83 MeV lying next above the 3.35-MeV level (Fig. 1). The ground-state transition from this level (not illustrated in Figs. 2–3) is observed to experience the maximum shift corresponding to an attenuation factor $F' = (1.09 \pm 0.12)$ from which we obtain a limit on the mean lifetime of the 3.83-MeV level of $\tau < 0.073 \times 10^{-12}$ sec, again to two standard deviations. In assigning the 3.83-MeV gamma ray to the $3.83 \rightarrow 0$ de-excitation, we have utilized the results of additional measurements[8] which show that the 3.83-MeV level de-excites to the ground state and to the 3.06-MeV level with branching ratios of 39% and 52%, respectively, and that the 3.73- and 3.79-MeV levels have weak or undetected[8] ground-state decays.

For the remaining four levels we obtain the indicated solutions for τ. These latter results are discussed more fully with respect to the line-shape analysis of the various transitions.

The 3.35-MeV Level of F^{18}

The experimentally determined line shape of the F^{18} $3.35 \rightarrow 0$ transition (second escape peak) is shown in Fig. 7(a). The points show the net spectrum (after subtraction of the fitted exponential background of Fig. 4) corresponding to the measurement for $\theta = 8°$. It has been constructed as the sum of the data for the two angles $\theta = 8°$ and $\theta = 172°$ through the following procedure. Since $\langle\cos\theta_1\rangle \equiv -\langle\cos\theta_2\rangle$ for the present experimental conditions, the spectrum measured for $\theta = 172°$ must, if reflected about the energy defined by $E_{\gamma 0}$, be identical to that measured for $\theta = 8°$. $E_{\gamma 0}$ has been defined precisely as a result of the centroid fitting procedure described previously. Also, visual inspection of the two curves, after reflection of one, readily provides a determination of the channel corresponding to $E_{\gamma 0}$ to an accuracy of better than a channel.

Thus, the spectrum of Fig. 7(a) was constructed by reflecting the 172° data about $E_{\gamma 0}$ and adding it to the 8° data to result in a curve with improved statistics.

TABLE I. Doppler-shift attenuation factors F' for gamma rays from $O^{16}(He^3, p\gamma)F^{18}$.

F^{18} transition	$\langle\Delta E_\gamma\rangle_{\text{expt}}$ (keV)	$\langle\Delta E_\gamma\rangle_{\text{calc}}$ (keV)	F'	v_i/v_0	τ (10^{-12} sec)
$1.045 \rightarrow 0$	9.47±1.0	14.9±3.3	>0.64±0.16	0.98±0.22	<0.5
$1.70 \rightarrow 0$	6.73±1.4	24.2±4.8	0.28±0.08	0.98±0.20	0.92±0.28
$2.10 \rightarrow 0.94$	1.15±0.3	16.6±3.1	0.07±0.02	0.98±0.18	4.4 ±1.6
$2.53 \rightarrow 0$	13.3 ±0.7	35.9±6.0	0.37±0.07	0.98±0.17	$0.61_{-0.15}^{+0.22}$
$3.06 \rightarrow 0$	45.0 +2.3	43.6±6.3	1.03±0.16	0.98±0.15	<0.17
$3.35 \rightarrow 0$	19.7 ±3.2	47.7±6.3	0.41±0.09	0.98±0.13	$0.52_{-0.14}^{+0.18}$
$3.83 \rightarrow 0$	59.7 ±1.2	54.5±5.7	1.09±0.12	0.98±0.10	<0.073

[8] J. W. Olness and E. K. Warburton, Bull. Am. Phys. Soc. **11**, 405 (1966); and to be published.

This procedure would also tend to reduce possible systematic errors arising from the subtraction of the fitted exponential background.

The decomposition of the resultant plot into a "stopped peak" at $E_{\gamma 0}$ and a "fast component" (which goes to zero at $E_{\gamma 0}$) is apparent from the figure. The ratio R extracted from these data is 0.21 which from Fig. 6 indicates a value $\alpha/\tau=1.16$ corresponding to a lifetime of $\tau=0.40\times10^{-12}$ sec. The solid curve shows the shape calculated from Eq. (10) using these values for R, α, and τ. The contributions of the fast and stopped components are indicated by the dashed curves. The fit in the region of $E_{\gamma 0}$ is satisfactory. However, for values of ΔE_γ corresponding to $v/v_i\cong1$ the computed curve fails to match the data points due to the exclusion from our considerations of those broadening effects due to the distribution of initial ion velocities. The effects of this broadening could be approximated in the present case by folding in a distribution function of width proportional to the uncertainty in v_i/v_0 (see column 5, Table I). We note, however, that the broadening effects must be most severe in the region of $v/v_i\cong1$, and hence do not appreciably affect the determination of the ratio R. This is illustrated by the dot-dashed curve of Fig. 7(a) which was calculated for the parameters indicated corresponding to a value $\tau=0.46\times10^{-12}$ sec. The latter curve fails to match the data points in the region of the stopped peak ($\Delta E_\gamma\cong0$), and the relative areas of the fast and stopped components are clearly in error. Hence the uncertainty to be assigned due to our ignorance of the initial velocity distribution is in this case appreciably smaller than in the line-shift analysis. The major uncertainty lies in the determination for the nuclear stopping power which, through the term γ_i strongly influences the values obtained for τ. For the present case then we obtain a value $\tau=(0.40\pm0.10)\times10^{-12}$ sec where the uncertainty arises, as stated, primarily from the latter source. This result compares favorably with the value $(0.52_{-0.12}{}^{+0.15})\times10^{-12}$ sec obtained from the Doppler shift attenuation method. Since the uncertainties associated with the two determinations are comparable, we take the average of these results to obtain $\tau=(0.46\pm0.12)\times10^{-12}$ sec. These results are summarized in Table II where we have listed the lifetimes obtained by the two methods together with the average of these values, and for comparison the values obtained in previous experiments.

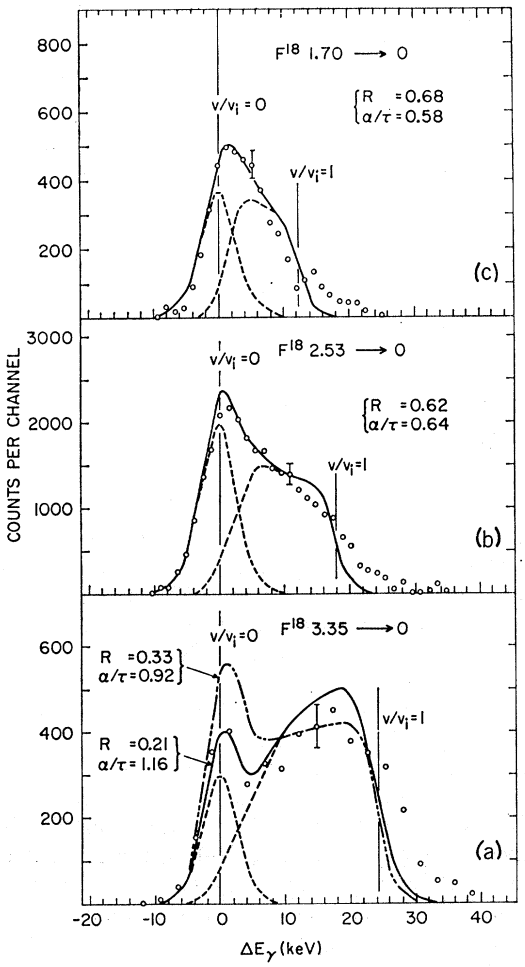

FIG. 7. A comparison of calculated line shapes with the experimental data for Doppler-shifted ground-state transitions from the 3.35-, 2.53-, and 1.70-MeV levels of F^{18}. The open circles show the experimental data on these transitions, taken from Figs. 2–3 and replotted on an expanded scale with an exponential background removed. The interesting parameter here is the ratio of the F^{18} ion velocity v to the initial ion velocity v_i [as determined by the kinematics of the $O^{16}(He^3,p\gamma)F^{18}$ reaction] since the Doppler shift ΔE is linear in $V\equiv v/v_i$. The solid curves are calculated, as explained in the text, for the indicated ratios of α/τ. The "slow" component centered at $v=0$ and the "fast" component, which extends into the region $v=v_i$, are also indicated. These calculated curves have been folded in with an $\sim$ Gaussian resolution function approximating the detector resolution. For the $3.35\rightarrow0$ transition the best fit is obtained for a value $\alpha/\tau=1.16$. The curve calculated with α/τ differing from this value by 20% is shown to illustrate the degree to which the line shape depends on the lifetime τ relative to the stopping time α.

The 1.70- and 2.35-MeV Levels of F^{18}

Similar results are shown in Figs. 7(b) and 7(c) for the ground-state transitions from the 2.53- and 1.70-MeV levels, respectively. The solid curves are the best fits calculated for the indicated values of the parameters R and α/τ. The values thus obtained for τ are summarized in column 3 of Table II. The lifetimes of these two levels are appreciably longer than that of the 3.35-MeV level, hence the relative intensity of counts in the stopped peak is greater. Because of the smaller transition energies the curves are "compressed" towards $E_{\gamma 0}$.

The 2.10-MeV Level of F^{18}

The attenuation factor $F'=(0.07\pm0.02)$ determined for the $2.10\rightarrow0.94$ transition corresponds to a mean lifetime $\tau=(4.4\pm1.6)\times10^{-12}$ sec. The data from which

TABLE II. Summary of lifetime determinations for bound levels of F^{18}.

Level in F^{18} E_{ex} (MeV)	Mean lifetime τ (psec) Present results Line shift	Line shape	Average	Previous results	Average
0.94				68 ±7[a]	68 ±7
1.045	<0.5		<0.5	<0.3[b]	<0.3
1.082				30 ±3[a]	30 ±3
1.125				(215 ±10)×10³[c]	(215 ±10)×10³
1.70	0.92±0.28	0.80±0.20	0.86±0.20	2 ±1[b]	0.9 ±0.2
2.10	4.4 ±1.6	3.8 ±1.5	4.1 ±1.6	5.3±3[a,d]	4.3 ±1.6
2.53	$0.61_{-0.15}^{+0.22}$	0.73±0.18	0.67±0.18	1.1±0.2[b]	0.9 ±0.2
3.06	<0.17		<0.17		<0.17
3.35	$0.52_{-0.14}^{+0.18}$	0.40±0.10	0.46±0.10		0.46±0.12
3.84	<0.073		<0.073		<0.073

[a] See Ref. 9. [b] See Ref. 3. [c] See Ref. 10. [d] T. K. Alexander (private communication).

these values were extracted, contained in Fig. 2, are shown on an expanded scale (with exponential background removed) in Fig. 8. The positions of the computer determined centroids corresponding to $\langle E_\gamma \rangle$ are indicated, as is the transition energy $E_{\gamma 0}$. The solid curve shows the approximately Gaussian shape which should be expected if $\tau(2.10) \gg \alpha$. The broadening of the experimental curves for $\theta = 172°$ and 8° on the low and high energy sides, respectively, is apparent in Fig. 8, and is furthermore in the proper sense to be associated with a nonzero attenuation factor, as indicated by the displacements of $\langle E_\gamma \rangle$ and $E_{\gamma 0}$. Figure 9 shows the sum of these two spectra, after reflecting the $\theta = 172°$ data about $E_{\gamma 0}$. The resultant curve has been fitted according to Eq. (10) with $R = 4.9$ and $\alpha/\tau = 0.12$, corresponding to a value $\tau = (3.8 \pm 1.5) \times 10^{-12}$ sec. This result is in quite satisfactory agreement with the value $\tau = (4.4 \pm 1.6) \times 10^{-12}$ sec obtained from the measured value of the centroid shift, and we adopt the average value given in column 4 of Table II.

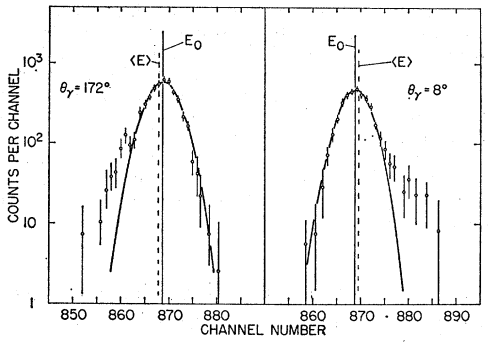

FIG. 8. Plots showing the Doppler-shift data on the 2.10 → 0.94 transition, on an expanded scale with an exponential background removed. The open circles show the experimental data, while the solid curves show the (symmetric) detector resolution function. The extent of the Doppler shift is indicated by the displacement of the average transition energy $\langle E \rangle$ relative to the unshifted transition energy E_0. Note that the "tails" observed for $\theta = 172°$ and $\theta = 8°$ are in the proper sense to be associated with a nonzero Doppler shift.

D. Discussion of Lifetime Measurements

The results of the present investigation have been summarized in Table II, which lists in column 4 the mean lives determined for the various levels indicated in column 1. For four of these levels the results of the line-shape analysis are given in column 3 for comparison with the results of the line-shift analysis given in column 2. Since there is good agreement, we have quoted the average values in column 4, noting, however, that these determinations are not independent. The results of other experimenters are collected in column 5 for comparison. With respect to the 1.045-, 1.70-, and 2.53-MeV levels the present results are in satisfactory agreement with the previous results of Litherland *et al.*[3] and we adopt the average values given in column 6.

The present value of $(4.1 \pm 1.6) \times 10^{-12}$ sec for the mean life of the 2.10-MeV level is in very good agreement with the value $(5.3 \pm 3) \times 10^{-12}$ sec reported by Alexander, Allen, and Healey.[9] We note that the lifetime of the 2.10-MeV level is such that it falls near the *upper* limit of the experimental sensitivity of the method used by Alexander *et al.*,[9] and conversely, at the *lower* limit of the present measurement. The lifetime is therefore restricted to lie in the small region of overlap corresponding to a value near 5×10^{-12} sec. Since the values established independently by the two experiments are in good agreement, we adopt the average value given in column 6.

The value $\tau = 0.7 \times 10^{-12}$ sec quoted previously[3] for the 2.10-MeV level has caused some difficulty in the interpretation of the decay of the 2.10-MeV level, particularly in regard to the transitions to the 0.937-MeV level ($J^\pi = 3^+$) and to the 1.082-MeV level (suspected $J = 0$). This will be discussed more fully in the later presentation of the correlation results. We note from Fig. 4 that the full-energy peak of the 2.10 → 0 transition is not completely resolved from the

[9] T. K. Alexander, K. W. Allen, and D. C. Healey, Phys. Letters **20**, 402 (1966), and also T. K. Alexander (private communication).

full-energy peaks of cascade transitions from the shorter lived 3.13- and 3.06-MeV levels. These levels were no doubt populated also in the $H^3(O^{16},F^{18})n$ reaction studied by Litherland *et al.*[3] with NaI(Tl) spectroscopy, in which case the shift measured for the $2.10 \rightarrow 0$ transition would have been in error due to the presence of these cascade components. This appears to be the most likely explanation of this previous[3] value obtained, which is clearly in error.

As a final consideration of these data, we note that, to two standard deviations, an upper limit of 3% can be placed on the branching ratios of the possible cascade transitions $2.10 \rightarrow 1.045$ and $2.10 \rightarrow 1.125$, as based on the absence of the corresponding peaks in the spectrum of Fig. 2. This limit on a possible $2.10 \rightarrow 1.045$ transition is more restrictive than that imposed previously by Chasman *et al.*[2]

The lifetimes of the first four excited states of F^{18} as determined by other authors[3,9,10] are also summarized in Table II for convenience. The lifetimes established for the 0.94- and 1.082-MeV levels by Alexander *et al.*[9] insure that the transitions from these levels have negligible Doppler shifts, as assumed in the energy calibrations of the present experiment. As these authors have pointed out,[9] the lifetime established for the 0.94-MeV level shows that the $E2$, $3^+ \rightarrow 1^+$ transition from the 0.94-MeV level is enhanced by a factor of ~ 6 over the single-particle Weisskopf estimate.[11] Their results also place a useful restriction on the amplitude of a possible $M3$ component as follows: Assuming an $M3$ strength corresponding to the most generous sum-rule limit for electric transitions,[11] namely $|M|^2 \leqslant Z^2$, we find the $M3/E2$ mixing ratio is restricted to values $|x| < 0.005$, where we have allowed for a variation in τ of 2 standard deviations from its measured[9] value. This is sufficiently small so that we may assume $x=0$ for this transition in the correlation analyses presented in the remainder of the paper.

III. PROTON-GAMMA CORRELATION MEASUREMENTS

A. Experimental Procedure

In the present paper we report on correlation measurements carried out at He^3 bombarding energies of 3.44 MeV using a singly ionized He^{3+} beam, and also at 4.65 and 5.40 MeV using a doubly ionized He^{3++} beam. These measurements were undertaken to study in particular the 2.10-, 3.13-, and 3.06-MeV levels of F^{18}—the bombarding energies were selected on the basis of yield curve measurements as being most favorable for the population of the states of interest.

The He^3 beam from the Brookhaven Van de Graaff accelerator was brought to a focus some 18 ft beyond the beam-analyzing magnet, where a collimating assembly restricted the beam to a $\frac{3}{32}$-in.-diam pencil. The collimator consisted of 5 equally spaced tantalum discs, separated by 3.5-in.-long lead cylinders with a $\frac{1}{4}$-in. central bore, all mounted in a 15-in. section of tubing. Beam definition was achieved by the first 4 discs with $\frac{3}{32}$-in. apertures, while the final disk with a slightly larger aperture served only to limit small angle scattering from the first four. The design of the collimator reflects the compromise dictated by the desire to pass as much beam as possible through the system for those experiments using the He^{3++} beam and the necessity for achieving a well-defined beam as required by the close geometry of the scattering chamber.

The scattering chamber itself was located 14 in. beyond the collimator assembly, and is shown schematically in Fig. 10. A liquid-nitrogen-filled cold trap located between these components served to reduce carbon buildup on slits and targets. The main body of the chamber was a 5-in.-diam brass cylinder to which were affixed the beam entrance and exit ports—also cylindrical. The alignment of their axes, and also the axis of the target holder, was achieved through the tolerances held in the machining process. After the detector was positioned on the detector mount, its distance from the target could then be varied by sliding the detector mount within the beam entrance port. A set of insulated tantalum apertures were used to insure that small-angle scatters from the primary collimating system could not possibly reach the detector, while the

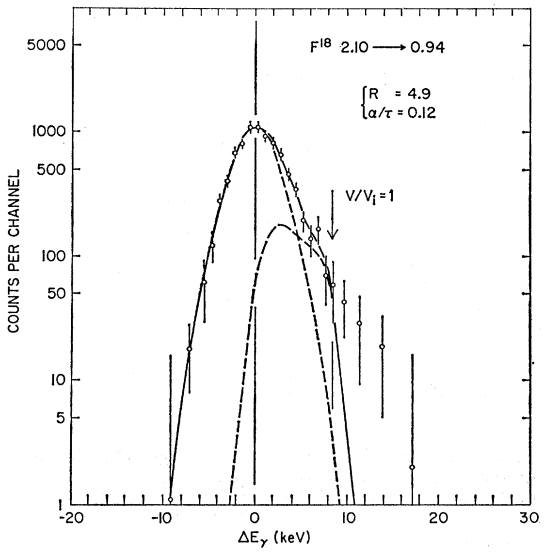

FIG. 9. A comparison of the calculated line shape with the experimental data for the Doppler-shifted $2.10 \rightarrow 0.94$ transition in F^{18}. The presentation is analogous to that of Fig. 7. The open circles show the experimental data, while the solid curve shows the line shape calculated for a ratio $\alpha/\tau = 0.12$, corresponding to a lifetime $\tau = (3.8 \pm 1.5) \times 10^{-12}$ sec. The "fast" and "slow" components of the calculated line shape are indicated by the dashed curves.

[10] A. R. Poletti and D. B. Fossan, Bull. Am. Phys. Soc. **11**, 368 (1966).

[11] D. H. Wilkinson, in *Nuclear Spectroscopy*, edited by F. Ajzenberg-Selove (Academic Press Inc., New York, 1960), Part B, p. 862 ff.

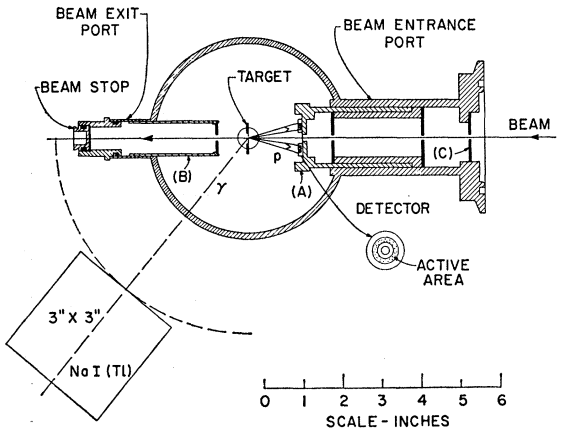

FIG. 10. Schematic illustration of the target chamber used in the present experiment for proton-gamma correlation measurements. Components not labeled are as follows: (A) Sliding detector mount. (B) Anti-backscatter shield. (C) Insulated tantalum apertures. The main body of the chamber was constructed of brass. However, the beam stop assembly and the antibackscatter shield were made of aluminum in order to reduce gamma absorption in the region $\theta_\gamma \sim 0°$.

current reading (normally zero) provided a check against gross misalignment of the beam.

After passing through the target the beam was stopped on a tantalum beam stop fixed to an aluminum plug fitted into the end of the beam exit port. The anti-back-scatter shield consisted of a $\frac{1}{8}$-in.-diam brass aperture fixed to a thin aluminum tube which was then positioned at a distance from the beam stop such that it was geometrically impossible for back-scattered particles to reach the annular detector. The targets were clamped to a rotatable centerpost projecting from the base of the chamber. The amount of this projection could be varied by a screw adjustment—hence it was practical to fix as many as 3 different targets at various distances along the projection axes, and then select the desired one by varying the projection distance.

The annular detector was obtained commercially and consisted of a 1.7-mm-thick disk of 12 000 Ω cm n-type silicon of 20 mm o.d. with an 8-mm hole which allowed the beam to pass. The active area was a ring 2.5 mm in width and 10 mm inner diameter. At a typical distance from the target (axial) of 4 cm the detector therefore subtended a mean angle of $\theta = 171°$ with a total spread of $\Delta\theta = 3.5°$.

Initial tests of the chamber were carried out using a 3×3-in. NaI(Tl) detector to record the photopeak counting rate from a Mn^{54} source placed at the target center. This permitted proper alignment of the gamma-detector axis with respect to the target center, and also permitted a direct check of nonsymmetry of the gamma-ray absorption effect due to the beam stop asesmbly. The results indicated that in this region of $-30° < \theta_\gamma < +30°$ the counting rate was reduced to ~90% of its value elsewhere. Since the thickness of the beam-collector assembly was already as small as practicable, this effect was reduced by adding a 1-mm layer of cadmium to the walls of the chamber corresponding to $|\theta_\gamma| > 30°$. In this manner the absorption correction in the region $\theta_\gamma \sim 0°$ was held to less than 2%. This of course applies to 847-keV gamma rays—for higher energy gamma rays the absorption effect will be smaller.

Targets were prepared by vacuum evaporation of SiO onto detergent-coated slides. The resultant films were floated onto water and affixed to thin tantalum holders with a $\frac{1}{4}$-in. hole, which were then clamped to the target post of the scattering chamber. The proton detector was positioned at an axial distance from the target of 4 cm, while the gamma detector, a 3×3-in. NaI(Tl) was placed at 15 cm from the target. The gamma-ray detector was shielded against general background radiation by 5 cm or more of lead.

Amplified coincidence pulses from the two detectors were analyzed by a TMC 16384-channel analyzer operating in a 256(gamma)×64(proton)-channel mode. Coincidence conditions were imposed by an external fast-slow coincidence circuit operating at a resolving time of ~0.06 μsec. A voltage gate set on an appropriate region of the proton detector spectrum provided a convenient monitor for the various correlation measurements, while the proton singles spectrum was simultaneously analyzed using a 400-channel RIDL analyzer. The results indicated that there were no significant gain shifts over the duration of the various coincidence measurements. At each of the selected bombarding energies measurements were made for 5 gamma-ray detection angles θ_γ; an additional measurement repeating one or more of these angles was used to check reproducibility of results. At each angle independent measurements were made of the proton- and gamma-singles spectrum, and of the ratio of randoms/reals which applied to the coincidence spectrum of interest. The results of these measurements were stored on magnetic tape for later analysis with an IBM 7094 computer. At the conclusion of the measurements for a given bombarding energy the data recorded at each angle were added together to obtain a sum spectrum, with improved statistics, which was useful in the determination of decay schemes and branching ratios.

The general features of the computer-implemented data handling procedure have been described previously.[12] Data corresponding to a given 2-parameter run are read from the magnetic tape into a matrix array corresponding to the original 256(gamma)×64(proton) channels of data storage. A matrix of randoms is then constructed from the proton- and gamma-singles spectra, normalized according to the experimentally determined ratio of randoms/reals, and then subtracted from the original data matrix to yield a 2-parameter spectrum corrected for chance coincidences. The gamma spectrum in coincidence with a given proton peak is

[12] See for example: E. K. Warburton and J. W. Olness, Phys. Rev. 147, 698 (1966).

then obtained, for example, by summing over the proton peak channels, and subtracting off a normalized "background" spectrum constructed by summing over near-lying background regions of the proton spectrum. The resultant gamma spectrum is then printed and plotted for inspection.

B. Results

The proton-detector pulse-height spectrum measured at a He^3 bombarding energy of 3.44 MeV is shown in Fig. 11. Proton groups from the $O^{16}(He^3,p)F^{18*}$ reaction are identified according to the level ordering of Fig. 1, and in some cases by the F^{18} excitation energy also. The expected position of groups p_1 and p_2 from the $C^{12}(He^3,p)N^{14*}$ reaction are also indicated. From their intensities, we conclude the target was relatively free of carbon contamination. The gamma-ray summed spectrum coincident with protons leading to the 2.10-MeV level of F^{18} is shown in Fig. 12. These data were obtained as the sum over all 9 of the individual correlation measurements performed at $E_{He^3}=3.44$ MeV. The gamma peaks all arise from de-excitation of the 2.10-MeV level, and are identified according to the initial and final levels between which each transition takes place. The inserts of Fig. 12 show portions of the individual spectra measured at $\theta_\gamma=0°$ and $\theta_\gamma=90°$. The "negative" peak at 0.511 MeV results from the randoms subtraction, reflecting the fact that the region $E_\gamma<0.55$ MeV was excluded from consideration in making this correction. This exclusion was necessary for the obvious reason that the amount of annihilation radiation present in any given spectrum did not follow the monitor counting rate, but depended on such factors as the initial positron activity at the beginning of each run and the total running time. We note, however, that the area of this negative peak is only $\sim 15\%$ of the area of the original 0.511-MeV peak before randoms

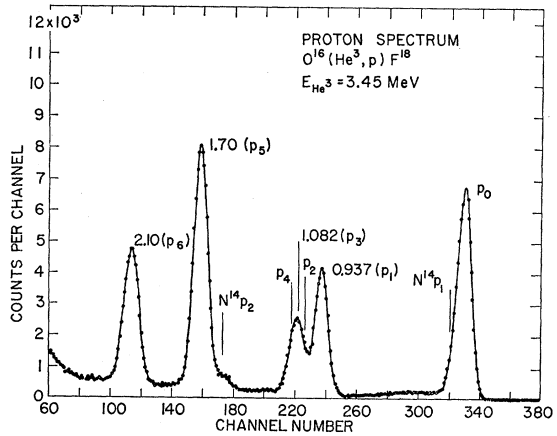

FIG. 11. Spectrum of protons from the $O^{16}(He^3,p)F^{18*}$ reaction measured with the annular detector (Fig. 10) at $E_{He^3}=3.44$ MeV. Proton groups from the above reaction are identified according to the level-ordering of Fig. 1. The position of proton groups p_1 and p_2 from the $C^{12}(He^3,p)N^{14*}$ reaction are also indicated.

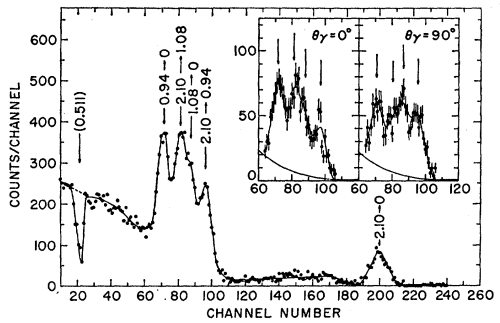

FIG. 12. Spectrum of gamma rays coincident with proton group p_6 (2.10-MeV level) from the $O^{16}(He^3,p\gamma)F^{18}$ reaction. These data are the sum of the 9 sets of data obtained at the 5 angles studied in the correlation measurements. The gamma rays resulting from de-excitation of the 2.10-MeV level are identified according to the excitation energies of the levels between which the transitions occur. The inserts show data taken at $\theta_\gamma=0°$ and $\theta=90°$. The solid curves are the results of a computer fit to these data to determine the relative intensities of the cascade gamma rays, and hence the p-γ correlations.

subtraction, thus indicating that the background counting rate did not change too drastically over the total time required for the 9 individual spectra comprising the sum spectrum of Fig. 12.

The results of similar analyses applied to these 2-parameter data, for $E_{He^3}=3.44$ MeV and also for $E_{He^3}=4.65$ and 5.40 MeV, are discussed in the following presentation of results for the levels of interest. Since our analysis of the correlation measurements is very similar to that described in detail by Poletti and Warburton,[1] we shall omit a lengthy discussion of the general procedure, and instead give reference to their publication.[1] In the following, as above, we discuss our results for the 2.10-MeV level in some detail as an example. Results for the remaining levels are then presented in a somewhat more summary form.

The 2.10-MeV Level of F^{18}

Plots similar to that shown in Fig. 12, showing the gamma spectra in coincidence with group p_6 (2.10-MeV level) were constructed from the data for each of the correlation angles. The angular dependence of the $2.10\rightarrow 0$ intensity was easily obtained by summing over the 2.10-MeV photopeak and normalizing these results to the monitor proton counts for each angle. These data were then fitted with an even-order Legendre polynomial expansion of the form $W(\theta)=I_\gamma\sum_\nu a_\nu P_\nu(\cos\theta)$. Solutions for the coefficients a_2 and a_4 ($a_0=1$) are given in columns 4 and 5 of Table III.

For the cascade transitions a different procedure was required, since the resolution of the 3×3-in. NaI(Tl) detector was not sufficiently good to resolve the 4 members of the $2.10\rightarrow 0.94\rightarrow 0$ and $2.10\rightarrow 1.08\rightarrow 0$ cascades. Instead we have used a Gaussian fitting program described previously[13] to fit the data for each

[13] See for example: J. W. Olness, E. K. Warburton, D. E. Alburger, and J. A. Becker, Phys. Rev. 139, B512 (1965).

TABLE III. Results of analysis of correlation data for the 2.10-MeV level of F^{18}.

Transition	E_γ[a] (MeV)	I_γ	a_2	a_4
2.10 → 0	2.102	91.3±3.1	−0.48±0.07	0.02±0.06
2.10 → 0.94	1.165	82.1±2.8	−0.12±0.07	0.04±0.07
1.08 → 0	1.082	80.5±2.8	−0.07±0.07	0.06±0.07
2.10 → 1.08	1.021	79.8±2.9	+0.60±0.08	−0.37±0.07
0.94 → 0	0.937	81.0±2.8	+0.21±0.07	−0.05±0.07

[a] Transition energies are taken from the results of Chasman *et al.*, Ref. 2.

angle and thus determine the relative intensity of each of these four components. This procedure was possible because of the following: (1) the lifetime of the 2.10-MeV level is sufficiently long (as determined in the previous section) that the various transitions experience Doppler shifts that are insignificant for the present considerations, (2) the energies of these transitions are thus very accurately known from the measurements of Chasman *et al.*[2] and also from the present Ge(Li) measurements. Therefore, since the relative peak positions are fixed, as are the relative peak widths, the fitting program need determine only 6 parameters: (1) a best peak width, (2) a best peak placement, and (3) the areas corresponding to the 4 line intensities. Two of the fits, for $\theta_\gamma=0°$ and $\theta_\gamma=90°$ are shown in the inserts of Fig. 12. Two different backgrounds were tried: parabolic and exponential, which were fitted to the regions above and below the quartet of lines. A comparison of these results indicated the line intensities thus determined were relatively insensitive to the exact form of the assumed background.

The intensities determined from the fitting procedure are plotted in Fig. 13. The points at 0°, 45°, 60°, and 90° each represent the average of two measurements which were found to agree with each other. The curves show the results of a Legendre polynomial fit to these data; the coefficients a_2 and a_4 determined thusly are summarized in Table III. The third column of Table III summarizes the relative intensities thus determined for the 5 transitions observed. The individual members of the two cascades 2.10 → 0.94 → 0 and 2.10 → 1.08 → 0 are equal within their errors, thus providing some further assurance that the fitting procedure is valid. From these data we determine branching ratios for transitions from the 2.10-MeV level to the ground-, 0.94-MeV, and 1.08-MeV states of 36±2, 32±2, and 32±2, respectively.

The correlation data summarized in Table III were next analyzed in order to see what restrictions could be placed on the allowable spins of the 2.10- and 1.08-MeV levels, and on the mixing ratios of the de-excitation gamma rays from the 2.10-MeV level. The method of analysis has been described in detail by Poletti and Warburton.[1]

These authors had determined previously that the spin of the 2.10-MeV level was either 1 or 2. Our present results for the 2.10 → 1.08 correlation, which exhibits a significant nonzero term in $P_4(\cos\theta)$, therefore determines that the 2.10-MeV level has $J=2$. The minimum value of χ^2 for a fit to the 2.10 → 1.08 correlation data, under the assumption $J=1$ for the 2.10-MeV level, is 9.4. Note that this result is not dependent on the spin (0, 1, 2) assumed for the 1.08-MeV level. Thus the possibility $J=1$ has been excluded with a confidence of better than 99.9%.

Figure 14 presents the results of a simultaneous fit to the correlation data for the members of the 2.10 → 0.94 → 0 cascade. The known spins and parities are given by the insert as is also the character of the 0.94 → 0 transition which is known to be $E2$. The curves are plots of χ^2 versus arctan$x$, where x is the unknown mixing parameter of the 2.10 → 0.94 transition. For discrete values of arctan$x$ between −90° and +90° (i.e., $-\infty \leq x \leq +\infty$), the allowable population parameters $P(\alpha)$ were adjusted to obtain a best fit to the correlation data and hence a minimum value of χ^2. The solid curve was computed under the assumption that only the $\alpha=0$ and $\alpha=1$ substates are populated, which would be true if the proton detector subtended a negligible solid angle at $\theta=180°$. The dashed curve shows our estimate of the maximum finite-size effect (FSE) which was obtained as the minimal envelope of curves calculated (a) with $P(2)=0.05P(0)$ and (b) with

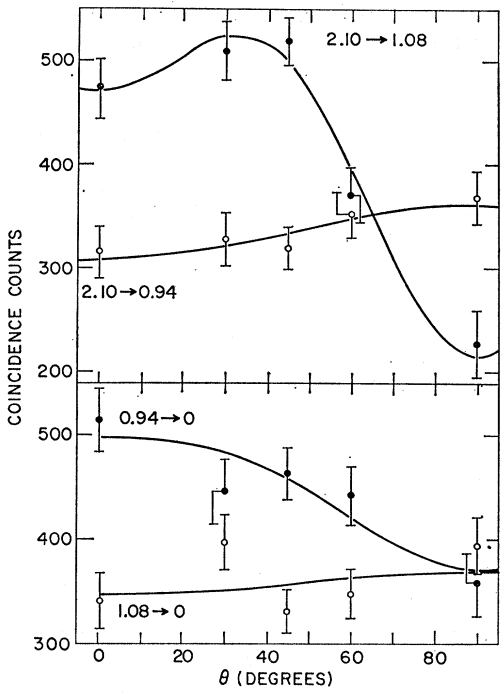

FIG. 13. Proton-gamma correlations for cascade transitions from the 2.10-MeV level of F^{18} populated via the $O^{16}(He^3,p\gamma)F^{18}$ reaction. The open and closed circles show the experimental data, while the curves are the results of an even-order Legendre polynomial fit to the data of the form $W(\theta)=I_\gamma \sum_\nu a_\nu P_\nu(\cos\theta)$. The large term in $P_4(\cos\theta)$ observed for the 2.10 → 1.08 correlation establishes a spin assignment of $J=2$ for the 2.10-MeV level.

$P(2)=0.1P(1)$. The two solutions for the mixing ratio x, corresponding to the minima of Fig. 14, are $x=(0\pm0.14)$, and $x=+(6_{-2}^{+9})$.

Figure 15 shows a similar plot for a simultaneous fit to the correlation data for the $2.10\rightarrow0.94\rightarrow0$ and $2.10\rightarrow1.08$ transitions, assuming spins of 0, 1, and 2 for the 1.08-MeV level and with the mixing ratio of the latter transition variable. The $2.10\rightarrow0.94$ transition is here fixed as dipole, corresponding to the first solution evident in Fig. 14. The inclusion of the $2.10\rightarrow0.94\rightarrow0$ correlation data in the present analysis of the $2.10\rightarrow1.08$ correlation ensures that the population parameters $P(0)$ and $P(1)$ will be restrained in the fitting procedure to values consistent with the first set of data. [We note that the ratios $P(1)/P(0)$ corresponding to the two minima of Fig. 14 are (0.57 ± 0.17) for $x=0$ and (0.63 ± 0.13) for $x=6$. Since these ratios are equal within these errors the procedure described above is therefore valid regardless of which solution applies to the mixing in the $2.10\rightarrow0.94$ transition.] The results thus obtained for assumed spins of 1 and 2 for the 1.08-MeV level are shown by the curves, while the value of χ^2 for $J=0$ is also indicated. The results indicate an order of preference for possible spins of the 1.08-MeV level of 0, 1, and 2. Although the possibility $J=2$ is ruled against with $\sim90\%$ confidence, the data are not sufficiently restrictive to allow its rigorous exclusion. We note, however, that for either $J=1$ or $J=2$ the $2.10\rightarrow1.08$ transition must have a significant quadrupole admixture.

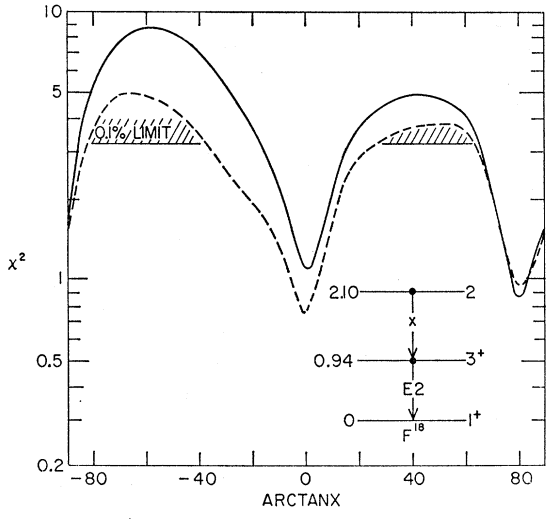

FIG. 14. Angular-correlation results for the F^{18} $2.10\rightarrow0.94$ transition. The solid curve shows a plot of χ^2 versus arctan$x$ for a simultaneous fit to the correlation data on the $2.10\rightarrow0.94$ and $0.94\rightarrow0$ cascade transitions. As indicated in the insert, x refers to the quadrupole/dipole mixing ratio in the $2.10\rightarrow0.94$ transition. The character of the $0.94\rightarrow0$ transition is taken to be effectively pure quadrupole, as explained in the text. The probability of χ^2 exceeding the value marked as the 0.1% limit is 0.1%. The dashed curve shows our estimate of the maximum possible finite-size effect (F.S.E.).

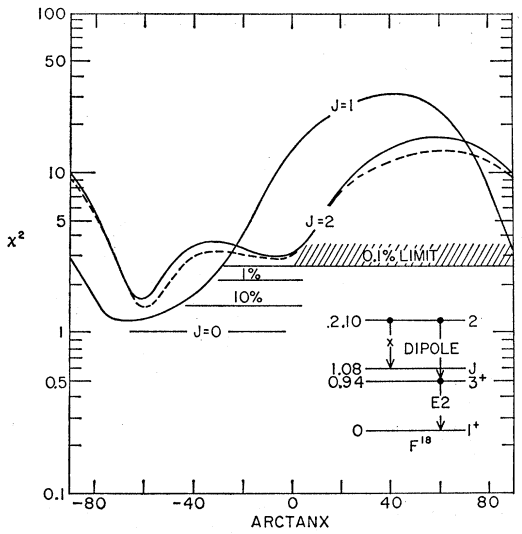

FIG. 15. Angular-correlation results for the F^{18} $2.10\rightarrow1.08$ transition. The plots show χ^2 as a function of arctan$x$ for assumed spins of $J=1$ and $J=2$ for the 1.08-MeV level. These results are obtained from a simultaneous fit to the correlation data on the three transitions indicated in the level-diagram insert. In this case x refers to quadrupole/dipole mixing in the $2.10\rightarrow1.08$ transition, with the $2.10\rightarrow0.94$ transition fixed as dipole, and the $0.94\rightarrow0$ transition as pure quadrupole. The dashed curve shows our estimate of the maximum possible F.S.E. for the curve corresponding to $J=2$. The value of χ^2 obtained for a $J=0$ assignment to the 1.08-MeV level is also indicated. The probability that χ^2 exceeds the values marked as 10%, 1%, and 0.1% are 10%, 1%, and 0.1%, respectively.

Following exactly the same procedure, a simultaneous fit to the $2.10\rightarrow0$ and $2.10\rightarrow0.94\rightarrow0$ correlations was made to determine the mixing in the ground-state transition. Two solutions are obtained, given by $x=+(0.11_{-0.11}^{+0.25})$ and $x=+(1.8_{-0.5}^{+0.7})$. This is unfortunately not as restrictive as the results obtained from a fit to the $2.10\rightarrow0$ correlation data alone, which yielded solutions $x=+(0.04_{-0.07}^{+0.3})$ or $+(1.95\pm0.35)$.

Figure 16 shows the results obtained from a simultaneous fit to the $2.10\rightarrow0$ and $2.10\rightarrow1.08$ correlation data for the purpose of determining the mixing ratio for the former transition. We have assumed the most likely spin, $J=0$, for the 1.08-MeV level in which case the $2.10\rightarrow1.08$ transition is pure quadrupole in nature. The solutions for the amplitude ratio of quadrupole/dipole radiation in the $2.10\rightarrow0$ transition then are $x=+(0.04\pm0.04)$ and $x=+(1.78\pm0.35)$. These results are somewhat more restrictive than those obtained from either of the two approaches described just previously, but hold only if $J=0$ for the 1.08-MeV level.

Table IV summarizes the information available on the gamma-branching of the 2.10-MeV level. Column 3 lists the branching ratios determined in the present work for transitions from the initial state (column 1) to the final states identified in column 2. The results of other investigators are summarized in column 4 for comparison. In view of the excellent agreement between

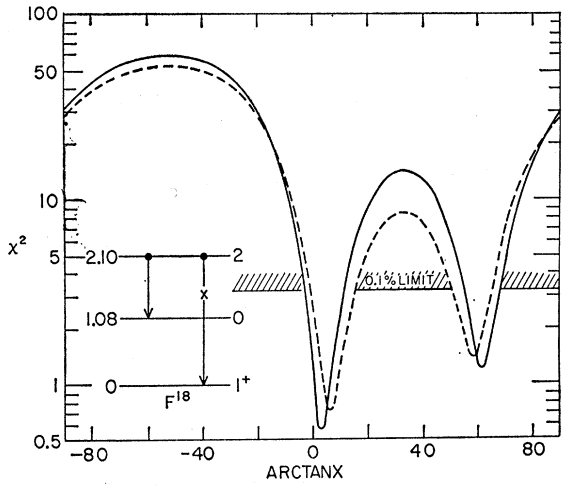

FIG. 16. Angular-correlation results for the F^{18} $2.10 \rightarrow 0$ transition. The curve shows χ^2 versus arctan$x$ for a simultaneous fit to the $2.10 \rightarrow 1.08$ and $2.10 \rightarrow 0$ correlation data to determine, in this case, the quadrupole/dipole mixing ratio of the latter transition. The 1.08-MeV level is here assumed to have spin 0 (most probable) in which case the $2.10 \rightarrow 1.08$ transition is pure quadrupole. The dashed curve shows our estimate of the maximum possible F.S.E.

the present results and those reported previously, we adopt the average values given in the last column.

The results presented thus far for the 2.10-MeV level are all based on the data obtained for $E_{He^3}=3.44$ MeV. From similar data obtained for $E_{He^3}=4.65$ MeV an analysis of the $2.10 \rightarrow 0$ correlation yields a solution for the mixing ratio of this transition of $x=+(0.04_{-0.07}{}^{+0.18})$ or $x=+(2.7\pm0.3)$. This is to be compared to the results summarized above which gave

TABLE IV. Summary of branching ratio determinations for levels of F^{18}.

Initial state (MeV)	Final state (MeV)	Branching ratios Present work	Previous work[a]	Average
1.70	0	28±3	35±3	32±3
	1.045	72±3	65±3	68±3
2.10	0	36±2	38±3	37±2
	0.937	32±2	30±5[b]	31±2
	1.045	<3	<6[b]	<3
	1.082	32±2	32±4[b]	32±2
	1.125	<3		<3
2.53	0	75±4	73±4	74±4
	0.937	21±4	23±2	22±4
	1.70	4±1.5	4±2	4±1.5
3.06	0	25±2	24±4	25±2
	0.937	75±2	76±4	75±2
3.13	0	32±2	31±3	32±2
	1.045	68±2	69±4	68±2
3.35	0	56±6	53±5	54±5
	0.937	7±4	4±4	5±3
	1.70	30±4	38±4	35±3
	2.10	7±4	5±4	6±3

[a] See Ref. 1.
[b] See Ref. 2.

$x=+(0.04_{-0.07}{}^{+0.3})$ or $x=+(1.95\pm0.35)$ and also to the solution of Poletti and Warburton which was $x=+(0.04\pm0.18)$ or $x=+(3.0\pm0.5)$. The weighted average of these results are $x=+(0.04_{-0.07}{}^{+0.18})$ or $x=+(2.5\pm0.3)$.

We now summarize the implications of the lifetime measurements (Table II) which determine a total width for the 2.10-MeV level of $\Gamma_\gamma=(1.5\pm0.5)\times10^{-4}$ eV. Combining this result with the branching ratios summarized in Table IV, we find the partial widths for transitions to the ground state and to the 0.94- and 1.08-MeV levels are $(0.6\pm0.2)\times10^{-4}$ eV, $(0.5\pm0.2)\times10^{-4}$ eV, and $(0.5\pm0.2)\times10^{-4}$ eV, respectively. We now consider these three transitions in order.

(1) The quadrupole/dipole mixing ratio for the $2.10 \rightarrow 0$ transition is either $x\sim0$ or $x\sim2.5$. If $x\sim0$, then the parity of the 2.10-MeV level may be either even or odd, since the computed dipole strengths are found to be reasonable in either case. For $x=2.5$ an odd parity assignment would require an $M2$ component of 11 ± 4 Weisskopf units (W.u.).[11] In view of the expected inhibition in self-conjugate nuclei of $\Delta T=0$ ML transitions,[14,15] this latter possibility may be rejected as unreasonably large. Conversely, the strength of the $E2$ component for an even parity assignment would be ~0.5 W.u.

(2) For the $2.10 \rightarrow 0.94$ transition the dipole strengths corresponding to the solution $x\sim0$ are consistent with either even or odd parity for the 2.10-MeV level. Again, the solution $x\sim6$ excludes an odd parity assignment, which would require an $M2$ component with $|M(M2)|^2\sim200$ W.u. For an even parity assignment, the $E2$ strength would be 9 ± 3 W.u. for $x=6$.

(3) For the $2.10 \rightarrow 1.08$ transition, these results show that the 2.10- and 1.08-MeV levels have the same parity, as follows. If, as expected, the spin of the 1.08-MeV level is $J=0$, then the $2.10 \rightarrow 1.08$ transition is pure $E2$, having a strength of $|M(E2|^2=(20\pm7)$ W.u. It is clear that the transition may not be $M2$.[14,15] If the spin of the 1.08-MeV level is either 1 or 2, then we have the restriction on the quadrupole/dipole mixing ratio (see Fig. 15) of $x>0.6$. This limit corresponds to a quadrupole strength of $|M(E2)|^2>6$ W.u. or $|M(M2)|^2>400$ W.u. The latter possibility can be firmly rejected, and thus we conclude that the 2.10- and 1.08-MeV levels have the same parity, since the transitions connecting them are either pure $E2$ (most likely) or a mixture of $M1/E2$ radiation.

In summary we conclude that the spin of the 2.10-MeV level is $J=2$, but the parity is not determined by these experiments. The 1.08-MeV level is most likely $J=0$, in which case the $E2$ $2.10 \rightarrow 1.08$ transition has a strength of (20 ± 7) W.u.

[14] E. K. Warburton, Phys. Rev. Letters **1**, 68 (1958).
[15] E. K. Warburton, in Proceedings of the Conference on Isobaric Spin in Nuclear Physics, Tallahassee, Florida, 1966 (to be published).

The 3.06-MeV Level of F^{18}

The gamma-ray spectra in coincidence with groups p_8 (3.06-MeV level) and p_9 (3.13-MeV level) are shown in Fig. 17. These data were obtained using a 5×5-in. NaI(Tl) detector at a He^3 bombarding energy of 4.65 MeV, for which it was found that the relative populations of the 3.06- and 3.13-MeV levels were $\sim\frac{2}{3}$. Similar data were also acquired at a bombarding energy of 5.40 MeV for which the relative populations were (3.06)/(3.13)$\sim$4/1. Figure 17 demonstrates the principal advantage which was gained by 2 parameter analysis of the p-γ coincidence data. Although the 3.06- and 3.13-MeV levels were not well resolved by the particle detector, the method of data reduction employed has provided a fairly clean separation of the gamma spectra associated with these 2 levels. Further, the small contribution to the 3.06-MeV spectrum due to the overlapping 3.13-MeV spectrum could be readily accounted for in the final analysis by observing, for example, the intensity of the 1.05-MeV transition due to the latter.

For these data the angular correlations of the ground-state and cascade gamma rays were easily extracted. Since the results of the individual analyses of the data at the two bombarding energies were in satisfactory agreement, we have chosen to present in the following an analysis of the total correlation data obtained for each transition by summing the correlation counting rates for each angle of the separate measurements. This is equivalent to studying the correlations corresponding to the weighted averages of the populations $P(0)$ and $P(1)$ actually obtained at the two bombarding energies. Table V summarizes the results of an even-order Legendre polynomial fit to these data of the form $W(\theta)=I_\gamma\sum_\nu a_\nu P_\nu(\cos\theta)$ with $\nu\leq\nu_{\max}$. The results of similar analyses for the data on other levels, to be discussed later, are also included. For each of the levels identified in column 1 solutions are listed for a_2 and a_4 determined by the fitting procedure for the transitions identified in column 2. For most cases the coefficient a_4 is statistically insignificant (as distinguished by the parentheses) and we give the value of χ^2 and the solution for a_2 obtained with $\nu_{\max}=2$. For the remainder (3 cases) the results refer to the fit obtained with $\nu_{\max}=4$.

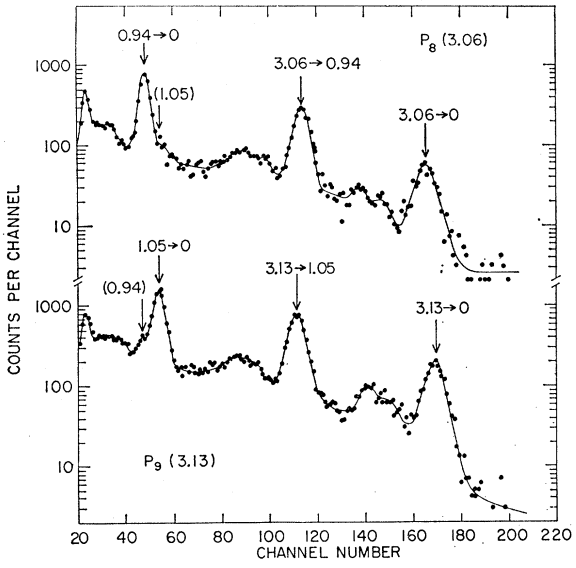

FIG. 17. Spectra of gamma rays coincident with protons populating the 3.06- and 3.13-MeV levels of F^{18} via the $O^{16}(He^3,p\gamma)F^{18}$ reaction. These spectra were obtained from 2-parameter data collected at a He^3 bombarding energy of 4.65 MeV. The extent to which the 2-parameter analysis has succeeded in separating the spectra from these two levels can be judged from the relative intensities of the 0.94- and 1.05-MeV peaks as observed in the two sets of data.

TABLE V. Results of an even-order Legendre polynomial fit to various correlation data from $O^{16}(He^3,p\gamma)F^{18}$.

Initial level (MeV)	Transition	a_2	a_4	χ^2
0.937	0.94 → 0	+0.35±0.12	−0.17±0.14	1.0
1.082	1.08 → 0	+0.06±0.13	(+0.14±0.15)	1.0
1.70	1.70 → 0	−0.33±0.05	(+0.05±0.05)	1.2
	1.70 → 1.05	−0.42±0.06	(+0.03±0.08)	1.0
2.53	2.53 → 0	−0.11±0.03	−0.44±0.03	0.9
	2.53 → 0.94	−0.37±0.08	(+0.08±0.09)	1.1
	0.94 → 0	+0.11±0.05	(−0.05±0.06)	0.9
3.06	3.06 → 0	−0.33±0.07	(−0.04±0.07)	1.0
	3.06 → 0.94	−0.17±0.05	(−0.06±0.05)	1.0
	0.94 → 0	+0.23±0.03	(−0.05±0.04)	1.3
3.13	3.13 → 0	−0.03±0.06	(−0.05±0.06)	0.8
	3.13 → 1.05	+0.26±0.03	(+0.02±0.04)	0.8
3.35	3.35 → 0	+0.07±0.07	−0.20±0.07	0.8
	(3.35 → 1.70 + 1.70 → 0)	+0.41±0.09	(+0.03±0.09)	1.0
	1.70 → 1.05	−0.20±0.07	(+0.04±0.07)	0.6

Our analysis of the correlation data for the 3.06-MeV level is summarized in Fig. 18. Analysis of the 3.06 → 0 transition (upper curve of Fig. 18) shows that the possibility $J=3$ for the 3.06-MeV level is excluded, in agreement with earlier work.[1] Possible assignments of $J>3$ would require $L\geq 3$ for the ground-state transition, which can be ruled out on the basis of the lifetime measurements of Sec. II which yielded $\tau(3.06)<0.17\times10^{-12}$ sec. For $L=3$, the 3.06 → 0 transition (24% branch) would have a strength $|M|^2>10^4$ W.u. which is clearly unreasonable. If $J=2$, as will be shown, then the solutions for x, the ratio of quadrupole/dipole radiation in the 3.06 → 0 transition, are $x=+(0.04\pm0.11)$ and $x=+(2.6\pm0.4)$, ignoring the FSE. Including our estimate of the possible FSE (the dashed curves of Fig. 18) results in solutions $x=+(0.04_{-0.11}{}^{+0.25})$ and $x=+(2.6_{-0.5}{}^{+0.4})$.

The lower curve shows the results obtained from a simultaneous fit to the correlation data for the indicated cascade transitions for assumed spins of 1 and 2 for the 3.06-MeV level. The possibility $J=1$ can now be

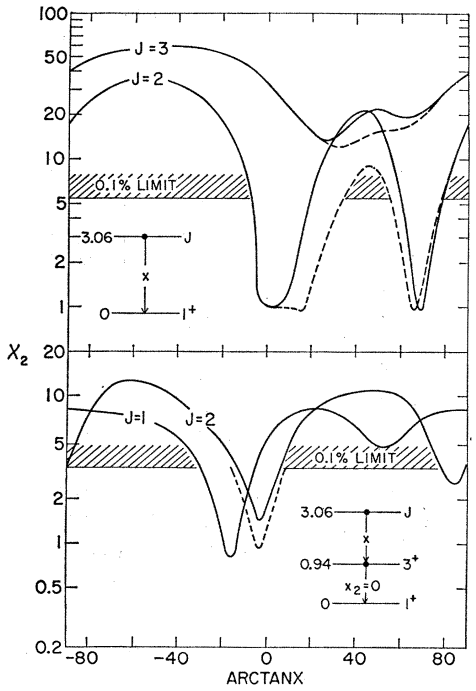

FIG. 18. Angular-correlation results for transitions from the 3.06-MeV level of F^{18}. The upper curves show plots of χ^2 versus arctan$x$ for $(L+1)/L$ mixing in the $3.06 \rightarrow 0$ transition for assumed spins of $J=2$ and $J=3$ for the 3.06-MeV level. It is thus clear that the possibility $J=3$ is ruled out with a confidence of better than 99.9%, since the minimum value of χ^2 for a $J=3$ assignment exceeds the indicated 0.1% confidence limit. The lower curve shows plots of χ^2 versus arctan$x$ for a simultaneous fit to the $3.06 \rightarrow 0.94$ and $0.94 \rightarrow 0$ correlation data, where x refers to $(L+1)/L$ mixing in the former transition. The $0.94 \rightarrow 0$ transition is here fixed as pure quadrupole. From these results, we see that a spin assignment $J=2$ for the 3.06-MeV level is consistent with the $3.06 \rightarrow 0.94$ transition being pure dipole. For a possible $J=1$ assignment, the $3.06 \rightarrow 0.94$ transition must have an appreciable octupole component which can be excluded on the basis of the lifetime measurements as given in the text.

excluded on the basis of the lifetime measurement, which restricts the octupole/quadrupole mixing ratio to values $|x|<0.063$, corresponding to $|\arctan x|<3.6°$. This restriction is based on the sum-rule limit[11] for electric transitions that $|M|^2 \leq Z^2$, and the further assumption that magnetic transitions cannot be stronger than electric transitions of the same order. From the results of Fig. 18 and using this restriction on $|x|$ we find that the possibility $J=1$ is ruled against with better than 99.9% confidence.

For $J=2$ the solution for the quadrupole/dipole mixing ratio is $x=-(0.06\pm0.06)$. The second minimum in χ^2 at $x=10.4$ is excluded from further consideration, since it dips to a confidence limit of only 3%, and further, since the lower limit on x for this minimum corresponds to a quadrupole component of $|M|^2 \gtrsim 30$ Weisskopf units, which we reject as unreasonably large.[14,15]

In summary, we conclude that the 3.06-MeV level has $J=2$ and the quadrupole/dipole mixing ratio for the $3.06 \rightarrow 0.94$ transition is $x=-(0.06\pm0.06)$.

The 2.53-MeV Level of F^{18}

We find that for the remaining levels of F^{18} the results of our present measurements are in agreement with those of Poletti and Warburton,[1] and hence serve primarily to confirm their conclusions. Accordingly, we present these results in summary form only. At the three bombarding energies used in the present measurements the levels studied were as follows: $E_{He^3}=3.44$ MeV (0.937, 1.082, 1.70, 2.10); $E_{He^3}=4.65$ MeV (2.10, 2.53, 3.06, 3.13, 3.35) and $E_{He^3}=5.40$ MeV (2.53, 3.06, 3.13, 3.35). The branching ratios thus determined for the various levels studied have been summarized in Table IV, while the measured correlations are given in Table V. Table VI summarizes the information thus obtained on multipole mixing in the ground-state transitions from the various levels studied. The excitation energy of the initial state and its spin are given in columns 2 and 3, while the bombarding energy at which the measurement was made is given in column 1. Column 4 lists the transitions which were fitted in the correlation analysis. For the 1.70- and 3.13-MeV levels the cascade transitions (of known multipolarity) to the 0^+ 1.045-MeV level have been included in the fitting procedure to determine the mixing in the ground-state transitions. Allowed solutions for these mixing ratios are summarized in column 5, while for comparison the results of Poletti and Warburton[1] are given in column 6. It is clear that the quoted uncertainties attached to the results listed in column 5 are generally larger than those of column 6; hence, the present results are not as restrictive as those given previously. Nevertheless, agreement between these two sets of measurements is good, and we therefore adopt the weighted average values summarized in column 7. These results will be discussed briefly in the following consideration of the individual levels.

The results of our analyses of the two sets of correlation data on the F^{18} 2.53-MeV level, obtained at He^3 bombarding energies of 4.65 and 5.40 MeV, are in satisfactory agreement, and hence we choose to discuss the combined data, as done previously for the 3.06-MeV level. We note that the angular correlations measured in the present experiment (see Table V) are very similar to those measured previously by Poletti and Warburton[1] at $E_{He^3}=4.0$ MeV. Hence the present analysis, which provides a rigorous confirmation of their conclusions, is also very similar. From a fit to the $2.53 \rightarrow 0$ correlation data possibilities $J \neq 2$ for the 2.53-MeV level are excluded with better than 99.9% confidence, in agreement with the conclusions of Poletti and Warburton. For $J=2$ we determine the quadrupole/dipole mixing in the $2.53 \rightarrow 0$ transition is $x=+(3.9_{-1.0}^{+0.8})$. This is in very good agreement with the result $x=+(3.5_{-0.75}^{+1.2})$ obtained previously,[1] and we adopt the average value given by $x=+(3.7\pm0.7)$. From the mean-life and branching ratios given in Tables II and IV we compute a total width $\Gamma_\gamma=(0.73$

TABLE VI. Mixing ratios for some ground-state transitions in F^{18}.

E_{He^3} (MeV)	Initial state (MeV)	Spin	Distributions fitted	x = Mixing ratio of $(L+1)/L$ radiation: Present work	Reference 1	Average
3.44	0.937	3^+	0.937 → 0	$+(0.07\pm0.15)$	$+(0.08\pm0.08)$	$+(0.08\pm0.07)$
3.44	1.082	2^a	1.082 → 0	$-(0.27\pm0.09)$, $+(7.6_{-3.6}^{+2.0})$	$-(0.23\pm0.07)$, $+(8.1_{-2.5}^{+6})$	$-(0.25\pm0.07)$, $+(8_{-2.5}^{+6})$
3.44	1.704	1^+	1.703 → 0	$+(0.58\pm0.16)$, $+(1.7\pm0.6)$	$+(0.49\pm0.06)$, $+(2.05\pm0.3)$	$+(0.50\pm0.06)$, $+(2.0\pm0.3)$
			+1.703 → 1.045			
3.44	2.103	2	2.103 → 0	$+(0.04_{-0.07}^{+0.3})$, $+(1.95\pm0.35)$	$+(0.04\pm0.18)$, $+(3.0\pm0.5)$	$+(0.04_{-0.07}^{+0.18})$, $+(2.5\pm0.3)$
4.65	2.103	2	2.103 → 0	$+(0.04_{-0.07}^{+0.18})$, $+(2.7\pm0.3)$		
4.65+5.40	2.53	2^+	2.53 → 0	$+(3.9_{-1.0}^{+0.8})$	$+(3.5_{-0.75}^{+1.2})$	$+(3.7\pm0.7)$
4.65+5.40	3.06	2	3.06 → 0	$+(0.04\pm0.11)$, $+(2.6\pm0.4)$		$+(0.04\pm0.11)$, $+(2.6\pm0.4)$
4.65	3.13	1	3.13 → 0	$+(0.13\pm0.13)$, $\lvert x\rvert>2.6$	$+(0.03\pm0.04)$, $\lvert x\rvert>10$	$+(0.04\pm0.04)$, $\lvert x\rvert>10$
			+3.13 → 1.045			

[a] Assumed.

$\pm0.16)\times10^{-3}$ eV and a partial width for the $2.53\rightarrow0$ transition of $(0.54\pm0.12)\times10^{-3}$ eV. The strength of the 94% quadrupole component is then calculated to be either (2.1 ± 0.3) or (48 ± 9) Weisskopf units, depending on whether the radiation is $E2$ or $M2$ in character, respectively. The latter possibility we reject, with a bit more firmness than was allowed previously,[1] and thus confirm the assignment $J^\pi=2^+$ for the 2.53-MeV level.

The correlation data on the $2.53\rightarrow0.94\rightarrow0$ cascade transitions were also investigated to see what restrictions could be placed on the $E2/M1$ mixing ratios for the $2.53(J^\pi=2^+)\rightarrow0.94(J^\pi=3^+)$ transition. The most definitive results were obtained upon inclusion of the $2.53\rightarrow0$ correlation data, with the mixing ratio of this latter transition fixed at the value $x=+(3.7\pm0.7)$ determined above. Our conclusions on the mixing in the $2.53\rightarrow0.94$ transition can be summarized as follows: (a) To a confidence of better than 99.9% we can say that x is negative, with the exception of the possibility $x=+\infty$, which is ruled against with only 90% confidence. (b) This transition has a nonzero quadrupole ($E2$) component. The lower limits on $|x|$, corresponding to confidence limits of 10%, 1%, and 0.1%, are respectively 0.31, 0.18, and 0.09. The corresponding lower limits on the $E2$ strength in Weisskopf units, are 1.0, 0.4, and 0.1, respectively.

The 3.35-MeV Level of F^{18}

At the bombarding energies used the proton group populating the 3.35-MeV level of F^{18} was unresolved from that populating the 5.69-MeV level of N^{14} via the $C^{12}(He^3,p)N^{14*}$ reaction. This latter reaction, unfortunately, gives rise to a gamma ray of energy 3.38 MeV which is energetically indistinguishable from the $3.35\rightarrow0$ transition in F^{18}. In view of the uncertainty attached to the unfolding of these two spectra, these data have not been included in the present analysis. We note, however, that the term in $P_4(\cos\theta)$ observed in the $3.35\rightarrow0$ correlation supports the conclusion $J\geqslant2$, and hence is in agreement with the results of Poletti and Warburton,[1] who deduced that $J=2$ or 3. Their conclusions on the mixing ratio of the $3.35\rightarrow0$ transition are summarized as follows: If $J=2$, then x is in the range $-4.7\leq x\leq-0.8$. If $J=3$, then $x=+(0.02\pm0.05)$ or $x=+(4_{-0.75}^{+1.1})$.

Figure 19 shows the results of a fit to the correlation data on the stronger cascade transitions from the 3.35-MeV level. The approach is identical to that discussed in detail by Poletti and Warburton, in which the angular variation in intensity of the unresolved $3.35\rightarrow1.70$ and $1.70\rightarrow0$ transitions and also of the $1.70\rightarrow1.05$ transition are fitted simultaneously to determine the mixing ratio of the $3.35\rightarrow1.70$ transition. The results presented in Fig. 19 show that we are unable to distinguish between the two allowed[1] possibilities $J=2$ and $J=3$.

We now combine the result of the lifetime deter-

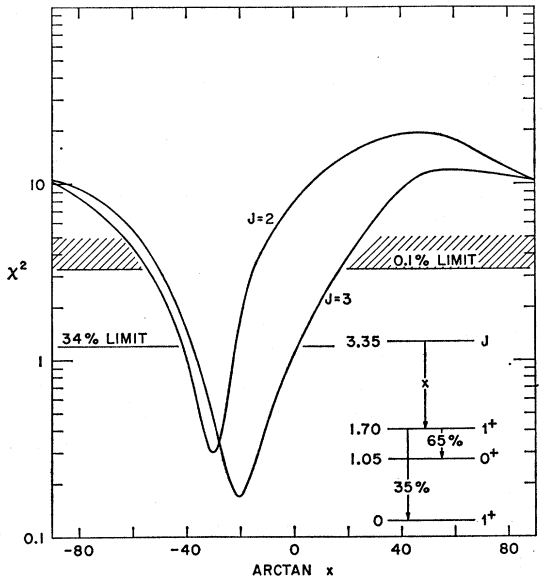

FIG. 19. Angular-correlation results for the F^{18} $3.35\rightarrow1.70$ transition, showing plots of χ^2 versus arctan$x$ for assumed spins of $J=2$ and $J=3$ for the 3.35-MeV level. In this case x refers to the $(L+1)/L$ mixing ratio in the $3.35\rightarrow1.70$ transition, which is unresolved from the $1.70\rightarrow0$ transition. These curves were obtained from a simultaneous fit to the correlation data for the $1.70\rightarrow1.05$ transition and to the net correlation data on the unresolved members of the $3.35\rightarrow1.70\rightarrow0$ cascade transitions. The 34% confidence limit, corresponding to one standard deviation in arctan$x$, and also the 0.1% confidence limit are indicated. For both $J=2$ and $J=3$ the F.S.E. was found to be negligible.

mination (Table II) with the branching ratios (Table IV) to compute the partial widths for gamma-de-excitation of the 3.35-MeV level. The results are $\Gamma_\gamma(3.35 \rightarrow 0) = (0.8 \pm 0.2 \times 10^{-3}$ eV and $\Gamma_\gamma(3.35 \rightarrow 1.70) = (0.6 \pm 0.1) \times 10^{-3}$ eV. We consider separately the two possible spin assignments for the 3.35-MeV level.

If $J=3$ the data are consistent with both the $3.35 \rightarrow 0$ and $3.35 \rightarrow 1.70$ transitions being pure quadrupole. For an even-parity assignment to the 3.35-MeV level, the $E2$ strengths for transitions to the ground state (1^+) and to the 1.70-MeV level (1^+) are computed to be (0.8 ± 0.2) W.u. and (19 ± 5) W.u., respectively. Conversely, if $J^\pi = 3^-$ for the 3.35-MeV level, the $3.35(3^-) \rightarrow 1.70(1^+)$ transition would be $M2$ of strength ~ 430 W.u. which can be firmly rejected.[14,15] Thus the 3.35-MeV level cannot have $J^\pi = 3^-$.

If $J=2$ for the 3.35-MeV level, the restriction on the mixing ratio for the $3.35 \rightarrow 0$ transition is[1] $-4.7 \leq x \leq -0.8$ and for the $3.35 \rightarrow 1.70$ transition, from Fig. 19, we have $-0.9 \leq x \leq -0.38$. Thus a 2^- assignment for the 3.35-MeV level would require that the $3.35(2^-) \rightarrow 1.70(1^+)$ transition have an $M2$ component (for $|x| > 0.38$) of strength $|M(M2)|^2 > 22$ W.u. (to two standard deviations in Γ_γ), which we reject as being quite unreasonable.[14,15] Conversely, for a $J^\pi = 2^+$ assignment to the 3.35-MeV level, the $E2$ component in the $3.35 \rightarrow 1.70$ cascade would have a strength of $(4.8_{-1.9}{}^{+4.0})$ W.u., where we have included the uncertainty due to the determination of x, while the strength of the $E2$ component in the $3.35 \rightarrow 0$ transition would be less than 1 W.u.

In summary then, we find the present data are in agreement with a spin-parity assignment of either $J^\pi = 2^+$ or $J^\pi = 3^+$ for the 3.35-MeV level. In either eventuality, the $3.35 \rightarrow 1.70$ transition has an appreciable $E2$ component, of strength $(4.8_{-1.9}{}^{+4.0})$ W.u. (if $J=2$) or (19 ± 5) W.u. (if $J=3$).

The 0.94-MeV Level of F^{18}

Our present results are consistent with the previous conclusion[1] that the 0.94-MeV level of F^{18} has $J^\pi = 3^+$. The value of the mixing ratio for possible octupole/quadrupole mixing in the $0.94 \rightarrow 0$ transition, based on these correlation measurements, is $x = +(0.08 \pm 0.07)$ (see Table VI). This is consistent with, but less restrictive than, the limitation $|x| < 0.005$ obtained from the lifetime measurement of Alexander *et al.*[9] as explained in Sec. II.

The 1.08-MeV Level of F^{18}

The correlation data for the 1.08-MeV level are consistent with a spin assignment of either 0, 1, or 2 for this level. If $J=1$ the possible quadrupole/dipole mixing in the $1.08 \rightarrow 0$ transition is not specified by these measurements, but if $J=2$ the mixing is restricted to the solutions for x given in Table VI. We note again that the most probable spin for the 1.08-MeV level is 0, as established from our analysis of the $2.10 \rightarrow 1.08$ correlation.

The 1.70-MeV Level of F^{18}

The present measurements confirm the findings of Poletti and Warburton[1] that the 1.70-MeV level has $J=1$. Solutions for the mixing ratio of the $1.70 \rightarrow 0$ ground-state transition, summarized in Table VI, are also in good agreement. We note that the revised lifetime given in Table II [$\tau = (0.9 \pm 0.2) \times 10^{-12}$ sec] for the 1.70-MeV level is approximately a factor of 2 shorter than that given previously,[3] and hence the possibility of an odd-parity assignment for the 1.70-MeV level is rejected even more firmly than before.[1] The strength of the $1.70 \rightarrow 1.045$ $M1$ cascade transition is found to be 0.09 ± 0.02 W.u.

The 3.13-MeV Level of F^{18}

We find that the 3.13-MeV level has $J=1$, in confirmation of the earlier conclusions of Poletti and Warburton.[1] The solutions obtained for possible quadrupole/dipole mixing in the $3.13 \rightarrow 0$ transition (see Table VI) are not as restrictive as those gotten previously[1] but the agreement is nevertheless satisfactory. (See note added in proof—Sec. IV.)

IV. DISCUSSION OF RESULTS

The present experiment has established uniquely spin assignments of $J=2$ for both the 2.10- and 3.06-MeV levels of F^{18}, and has suggested that an assignment of $J=0$ for the 1.08-MeV level is somewhat more likely than possible assignments of $J=1$ or 2. The parity of the 3.35-MeV level is established as even, while the 2.10- and 1.08-MeV levels have the same (but undetermined) parity. For the remaining levels—in particular the 0.94-, 1.045-, 1.70-, 2.53-, and 3.13-MeV levels—the present results are found to either confirm or substantiate previous conclusions on spins and parities as summarized schematically in Fig. 1. Branching ratios and multipole-mixing ratios determined from the present work are found to be in good agreement with the previous results of Poletti and Warburton[1] as summarized in Tables IV and VI. Similar studies of correlations in the $O^{16}(He^3,p\gamma)F^{18}$ reaction have very recently been reported by Chagnon.[16] We find the results summarized in the present paper in good agreement with his conclusions on the mixing ratios for ground-state transitions from the 2.10-, 2.53-, 3.13-, and 3.35-MeV levels, and also on the mixing in the $2.53 \rightarrow 0.94$ cascade transition. We note also that his results provide an independent confirmation of the spin assignments, or restrictions, advanced previously by Poletti and Warburton.[1] Points of disagreement arise with respect to the mixing ratio of the $3.35 \rightarrow 1.70$

[16] P. R. Chagnon, Nucl. Phys. **78**, 193 (1966).

transition. We note that the results of the present experiment are in agreement with those of Poletti and Warburton[1] for either of the possible assignments, $J=2$ or 3, for the 3.35 MeV level. For the $J=2$ possibility, the average of these two measurements yields a value for the $3.35 \rightarrow 1.70$ mixing ratio of $x=-(0.44 \pm 0.15)$. The solution obtained by Chagnon ($x<-7$) is in significant disagreement with this result, as mentioned previously.[16] We further note that a possible objection to a $J=0$ assignment for the 1.08-MeV level of F^{18}, as given therein,[16] has been removed by later work[17] in agreement with present results which tend to favor a $J=0$ assignment over $J=1$ or 2.

In summary, then, we note the following with respect to the low-lying levels of F^{18}: Of the ten levels below 3.4-MeV excitation in F^{18}, seven have received definite spin assignments, while for an eighth (the 1.125-MeV level) there is a strong theoretical preference for $J=5$. The possible spins of the remaining two levels have been restricted as indicated: 3.35-MeV level ($J=2$, 3) and 1.08-MeV level ($J=0$, 1, 2). There does not appear to be any strong theoretical preference for any of the alternative spin assignments to these two states.

Parity assignments have been established from experimental evidence for all but three levels. One of these, the 3.06-MeV level, is certainly of even parity, since the present assignment of $J=2$ to this level establishes it without doubt as the $J^{\pi}=2^{+}$, $T=1$ analog of the 2^{+} O^{18} first-excited state at 1.98 MeV, as set forth previously.[1,16] The parity of the 1.08- and 2.10-MeV levels are necessarily the same, since the transition connecting them is either pure $E2$ or an $E2/M1$ mixture. There does not appear to be any experimental evidence favoring either even or odd parity for these levels. However, if the 1.08-MeV level has $J=0$, as is most probable, then it would be difficult to reconcile an even-parity assignment with current theoretical models or systematics which do not predict a $J^{\pi}=0^{+}$, $T=0$ level at so low an excitation energy.

[17] P. R. Chagnon, Nucl. Phys. **81**, 433 (1966).

Of prime importance to the understanding of the F^{18} level structure therefore is the determination of the spin and parity of the 1.08-MeV level. The parity could be obtained indirectly by determining that of the 2.10-MeV level. In this respect we note that additional measurements on the $O^{16}(He^{3},p\gamma)F^{18}$ reaction disclose[8,18] states of excitation energy $3.4<E_{\text{exp}}<4.9$ MeV which are observed to de-excite through the 2.10 MeV level—but not to any appreciable extent through the 1.08-MeV level. These results suggest that while additional p-γ correlation measurements would be of value, it is likely that γ-γ triple correlation or alternately gamma-polarization experiments would be more suitable for the investigation of the parity of the 1.08-MeV level.

Note added in proof. Recent experiments have shown[17,18] that the F^{18} 1.08-MeV level has $J=0$ and that the 2.10-MeV level (and thus also the 1.08-MeV level) has odd parity.[19] It has also been found[20] that the 3.13-MeV level decays to both the 1.05- and 1.08-MeV levels with branching ratios of $(41\pm4)\%$ and $(27\pm4)\%$, respectively (instead of 68% to the 1.05 MeV level alone). This latter result does not affect the analysis of the 3.13-MeV level as presented in this and previous work[1,16] since both the 1.05- and 1.08-MeV levels have $J=0$.

ACKNOWLEDGMENTS

We would like to acknowledge various illuminating discussions with Dr. T. K. Alexander and Dr. R. M. Freeman on this problem, and to thank these authors and also Dr. P. R. Chagnon for communicating their results prior to publication. We would especially like to thank Dr. Alexander for first pointing out to us the evidence contained in our data for a nonzero Doppler shift of the de-excitation gamma rays from the F^{18} 2.10-MeV level.

[18] S. Gorodetzky, R. M. Freeman, A. Gallmann, F. Haas, and B. Heusch (to be published).

[19] A. R. Poletti, Phys. Rev. (to be published).

[20] E. K. Warburton, J. W. Olness, and A. R. Poletti (to be published).